General Disclaimer

One or more of the Following Statements may affect this Document

- This document has been reproduced from the best copy furnished by the organizational source. It is being released in the interest of making available as much information as possible.

- This document may contain data, which exceeds the sheet parameters. It was furnished in this condition by the organizational source and is the best copy available.

- This document may contain tone-on-tone or color graphs, charts and/or pictures, which have been reproduced in black and white.

- This document is paginated as submitted by the original source.

- Portions of this document are not fully legible due to the historical nature of some of the material. However, it is the best reproduction available from the original submission.

Produced by the NASA Center for Aerospace Information (CASI)

NASA TECHNICAL MEMORANDUM

NASA TM-73856

NASA TM-73856

(NASA-TM-73856) SELF-ACTING SHAFT SEALS (NASA) 36 p HC A03/MF A01 CSCL 11A

N78-19513

Unclas
G3/37 08679

SELF-ACTING SHAFT SEALS

by Lawrence P. Ludwig
Lewis Research Center
Cleveland, Ohio 44135

TECHNICAL PAPER to be presented at the
AGARD Power, Energetics, and Propulsion Panel Meeting
on Seal Technology in Gas Turbine Engines
London, England, April 6-7, 1978

SELF-ACTING SHAFT SEALS

Lawrence P. Ludwig
National Aeronautics and Space Administration
Lewis Research Center
Cleveland, Ohio 44135

E-9446

SUMMARY

Self-acting seals are described in detail. The mathematical models for obtaining a seal force balance and the equilibrium operating film thickness are outlined. Particular attention is given to primary ring response (seal vibration) to rotating seat face runout. This response analysis reveals three different vibration modes with secondary seal friction being an important parameter. Leakage flow inlet pressure drop and affects of axisymmetric and nonaxisymmetric sealing face deformations are discussed. Experimental data on self-acting face seals operating under simulated gas turbine conditions are given; these data show the feasibility of operating the seal at conditions of 345 N/cm^2 (500 psi) and 152 m/sec (500 ft/sec) sliding speed. Also a spiral groove seal design operated to 244 m/sec (800 ft/sec) is described.

SYMBOLS

B	constant = $h_m - \frac{\alpha(r_o - r_i)}{2}$
F	sealing dam force, N; lbf
h	film thickness, cm; in.
h_{char}	characteristic film thickness = $(h_1^2 h_2^2 / h_m)^{1/3}$, cm; in.
ℓ	primary seal radial length
L	sealing dam circumferential length, cm; in.
M	Mach number
P	pressure, N/m^2 or N/cm^2; psi
ΔP	pressure difference, N/m^2 or N/cm^2; psi
Q	net leakage (volume) flow rate, scmm; scfm
R	radius, cm; in.
ΔR	sealing dam radial width, $R_o - R_i$, cm; in.
R	gas constant, universal gas constant/molecular weight
Re	Reynolds number
r	radial direction coordinate
T	temperature, K; ^oF
V	velocity, m/sec; ft/sec
x	coordinate in pressure gradient direction (radial direction)
y	coordinate across film thickness
z	shear flow coordinate in Cartesian system
α	relative inclination angle of primary seal faces, rad
β	axisymmetric relative inclination of primary seal faces, rad
γ	nonaxisymmetric relative inclination of primary seal faces, rad
μ	absolute or dynamic viscosity, $N\text{-}sec/m^2$; $(lbf\text{-}sec)/ft^2$
ρ	density, kg/m^3; $(lbf)(sec^2)/ft^4$

Subscripts:

av	average
char	based on characteristic film thickness
h	based on film thickness
i	inner cavity
m	mean
o	outer cavity
r	based on radius
s	spring
1	sealed pressure, upstream reservoir pressure
2	pressure at and within sealing gap inlet

ORIGINAL PAGE IS
OF POOR QUALITY

3 pressure at and within sealing gap exit

4 downstream reservoir pressure

INTRODUCTION

The continuing increases in gas pressure and temperature which accompany the evolution of the gas turbine, industrial compressor, and other rotating machinery places burdens on a shaft seal technology, which seems to some to be barely adequate for current needs. In addition, the emphasis on efficiency caused by the impending fuel shortage causes an additional need for seals with reduced leakage rates. In the gas turbine shaft seals are used to restrict leakage from a region of a gas at high pressure to a region of gas at a lower pressure and to restrict gas leakage into the bearing sumps. (Bearing sumps contain an oil-gas mixture at near ambient pressure, and gas leakage through the seal helps prevent oil leakage out and maintains a minimum sump pressure necessary for proper scavenging.) Bearing sumps in the high pressure turbine area are usually the most difficult to seal because the pressures and temperatures surrounding the sump can be near compressor discharge conditions.

Labyrinth seals are commonly used for shaft sealing in gas turbine engines (a simplified model of one system is shown in Fig. 1). The advantage of labyrinth seals is that the speed and pressure capability is limited only by the structural design; one disadvantage is a relatively high leakage rate. This leakage cam be a significant performance penalty, and will provide easier passage of air-borne water and dirt into the sump. In this regard high leakage rates of hot gas into the bearing compartment tend to carry oil overboard and add significantly to the heat dissipation burden of the oil cooling system. An added complication in small engines is the limited space available for seals and bearing sumps, here the multiple labyrinth seal with associated bleed and venting passages is difficult to accommodate.

Conventional rubbing contact seals, shaft riding and radial face types, are also used for sealing bearing sumps. Because of wear rate, shaft riding and circumferential seals (see Fig. 2 for one version), have been limited to pressure less than 69 N/cm^2 (100 psi); and successful operation has been reported at a sealed pressure of 58 N/cm^2 (85 psi), a gas temperature of 644 K (700° F), and a sliding velocity of 73 m/sec (240 ft/sec)(Ref. 1). On the other hand, the conventional rubbing contact face seal (Fig. 3) is limited to approximately 90 N/cm^2 (130 psi) and 122 m/sec (400 ft/sec) for long operational life. Rubbing contact seals are attractive because they have lower leakage rates than labyrinth seals. Associated with this lower gas leakage rate is less entrained debris, lower heat dissipation requirement for the oil cooling system, and lower efficiency penalty.

By incorporating thrust bearing geometry into a conventional face seal, nonrubbing operation can be achieved. This seal concept has been termed the "self-acting" seal, since the mechanism is similar to a self-acting thrust bearing in that the mating faces lift out of contact because of the pressure developed by relative motion between the seal faces. Studies (Refs. 2 and 3) demonstrated that the self-acting seals can operate at advanced aircraft engine conditions, that they have lower leakage rates than labyrinth seals, and hence that they are attractive from an efficiency standpoint.

The objectives of this paper are to (a) review the operating principle and design of the self-acting seal, (b) point out effects of adverse operating conditons, and (c) present some experimental data. The data are for two seal sizes, a 16.76-cm (6.60-in.) nominal diameter seal suitable for large gas turbines and a 6.44-cm (2.54-in.) diameter seal for small engines. The experimental portion of the program was run in rigs which simulated the bearing compartments of gas turbines, this placed the sealed pressure at the seal inside diameter; thus the bearing oil/air mixture was at the seal outside diameter and centrifugal force acted against oil leakage.

DISCUSSION AND ANALYSIS

Self-Acting Face Seal Terminology

The terms "hydrodynamic" and "hydrostatic" are often applied to describe seals for compressible fluids as well as for incompressible fluids. But following the bearing terminology, the terms "self-acting" and "pneumostatic" will be used when the sealed fluid is compressible, and the terms "hydrodynamic" and "hydrostatic" will be reserved for sealing incompressible fluids.

It should be noted that conventional "contact" seals often operate with separation of the sealing surfaces because of forces produced by self-acting, pneumostatic, hydrodynamic, or hydrostatic effects. This is particulary true in conventional radial face seals for liquids (such as pump seals), the hydrodynamic forces being produced by miniscule misalignments and surface waviness (which are largely unplanned and occur by happenstance) caused by such effects as local thermal expansions, friction, and wear. In contrast, in the seals which are the subject of this paper, the self-acting or hydrodynamic action is produced by a "machined in" bearing geometry and not by uncontrolled effects. Figure 4 shows this type of self-acting seal. (Since a hydrodynamic seal assembly would be the same in principle, the discussion can be limited to the self-acting seal.)

As previously mentioned, a self-acting face seal is similar to a conventional face seal except for the added feature of a self-acting geometry (gas lubricated thrust bearing). As with a conventional face seal, it consists of a rotating seat which is attached to the shaft and a nonrotating primary ring assembly which is free to move in an axial direction; thus the seal can accommodate axial motion such as is due to engine thermal expansion. The secondary seal (piston ring) is subjected only to the axial motion (no rotation) of the primary ring assembly. Several springs provide mechanical force to maintain contact at start and stop. In operation, the sealing faces are separated a slight amount (in the range of 2.5 to 1.27 μm (0.0001 to 0.0005 in.)) by action of the self-acting lift geometry. This positive separation results from the balance of seal forces and the gas film stiffness of the self-acting geometry. The self-acting geometry can be any of the various types used in gas thrust bearings; the Rayleigh step bearing is illustrated in Figs. 4 and 5.

Within the seal industry there is a wide variety of terms used to describe similar seal parts. The ASLE seal glossary (Ref. 4) has provided some guidance in seal nomenclature, and the self-acting nomenclature which follows is mainly an extension of this ASLE work. The nomenclature applying to an assembly of parts (Fig. 4) is

1. Primary seal - Seal formed by the sealing faces of the seat and primary ring. Relative rotation occurs between these sealing faces.
2. Secondary seal - Seal formed by the sealing surfaces of the secondary ring. In the case of a bellows seal the secondary seal is the bellows itself.
3. Static seal - Seal formed by the mating surfaces of the primary ring and its carrier (in some designs the static seal is an interference fit).
4. Self-acting geometry - Lift-pad geometry (Rayleigh step bearing) and mating face which together produce the thrust bearing action to separate the sealing surfaces.
5. Film thickness (h) - Distance between primary sealing faces or between surfaces forming the self-acting geometry. For parallel surfaces the film thickness at the primary seal is the same as at the self-acting geometry. (Note that h may vary with radial and circumferential position and with time.)
6. Seal head - Assembly that is axially movable and consisting of primary ring, its retainer (if any), and its carrier. (The retainer and the carrier are combined into one part in some designs.)

The nomenclature applying to single parts (Fig. 4) is

1. Seat - Part having a primary sealing face and mechanically constrained with respect to axial motion.
2. Primary ring - Part having a primary sealing face and not constrained with respect to axial motion.
3. Secondary ring - Part having secondary sealing surfaces which mate to the secondary sealing surfaces of the carriers.

Force Balance

General description. - To determine film thicknesses and leakage in a self-acting seal, the axial forces acting on the seal head (assembly of the primary ring and its carrier) must be determined over the range of operating conditions. These forces comprise the self-acting lift force, the spring force, and the pneumatic force due to the sealed pressure. Essentially, the analysis requires finding the film thickness for which the opening forces balance the closing forces. When this equilibrium film thickness is known, the leakage rate can be calculated. This force balance analysis is readily obtained for the steady-state case in which the seat face has zero runout with respect to the shaft centerline. In this regard, a complicating factor is seat face runout which introduces dynamic film thickness changes. (This is discussed in a later section.) For most seal design purposes the steady-state solution is sufficient.

The following sections outline the analysis used to obtain seal performance predictions over the operating range; for aircraft gas turbines this range is spanned by the idle and takeoff seal pressures, temperatures, and sliding speeds. To provide an example, the 16.76-cm (6.60-in.) diameter seal was selected for illustrating the performance prediction analysis. Also, for comparison purposes, the performance maps are given for a 6.44-cm (2.54-in.) diameter seal.

Primary Seal Pressure Gradient

To establish the axial force balance of the primary ring, the pressure gradient in the primary seal must be determined. (See Fig. 4 for primary seal location.) The mathematical models described in Refs. 5 to 7 were used for these calculations. From a gas leakage flow standpoint the primary seal is a long passage. For example, a typical operating film thickness of a self-acting seal is in the range of 10.2 μm (0.0004 in.), and a typical radial length of the primary seal is 0.127 cm (0.050 in.). Thus, the length to height (ℓ/h) ratio of the flow channel is in the range of 125/1. Data from Refs. 6 and 7 show that this leakage passage has the following qualitative features:

1. Laminar leakage flow prevails over much of the range of interest in seals for gas turbines (pressure range of 345 N/cm^2 abs (500 psia)).
2. Sonic velocity (choking) can exist at the passage exit for some of the larger pressure ratios and film thicknesses which occur in seal operation.
3. Pressure profiles across the primary seal for choked and nonchoked flow can be very different.
4. Since the primary seal radial width is small compared with its diameters, the area expansion effect on flow can be ignored.
5. The leakage flow and pressure profile are significantly different if the surfaces of the primary seal are not parallel. (See Ref. 8 for a discussion of the effects of converging and diverging sealing surfaces.)

The primary seal mathematical model used in the one-dimensional analysis of Refs. 5 and 7 is shown in Fig. 6. As mentioned, the area expansion effects are ignored, and the model is a passage of height h and length ℓ.

From stagnation source conditions of P_1 and V_1 (see Fig. 6) an isentropic expansion is considered to occur ahead of the entrance to the primary seal gap. Thus, the entrance pressure, P_2, is less than the stagnation pressure P_1, and the entrance velocity, V_2, is a finite value. To account for entrance loss and viscous friction, it was found necessary to use an entrance loss coefficient. Thus, the entrance velocity, V_2, is less than that calculated by isentropic expansion. In a later section the entrance effects are discussed in more detail.

Flow in the sealing gap is assumed one-dimensional and a friction factor is introduced to account for viscous losses. At the exit, three conditions are considered in the analysis: First, exit velocity, V_3, is subsonic and exit pressure, P_3, is equal to reservoir pressure, P_4. Second, exit velocity, V_3, is sonic and exit pressure, P_3, is equal to reservoir pressure, P_4. And third, exit velocity, V_3, is sonic, the flow is choked, and exit pressure, P_3, is greater than the reservoir pressure, P_4.

ORIGINAL PAGE IS
OF POOR QUALITY

If the flow is subsonic throughout, the analysis reduces to the following equations:

a. Leakage flow rate

$$Q = \begin{Bmatrix} 2.726 \\ 0.001287 \end{Bmatrix} \frac{h_{char}^3 L(P_1^2 - P_4^2)}{\mu RT(R_o - R_i)} \begin{Bmatrix} \text{scfm} \\ \text{scms} \end{Bmatrix} \tag{1}$$

b. Pressure distribution

Parallel film case

$$P = P_4\left[1 - \left(1 - \frac{P_1^2}{P_4^2}\right)\left(\frac{R_o - r}{R_o - R_i}\right)\right]^{1/2} \tag{2}$$

Small deformation case

$$P = P_1\left(1 + \frac{\left[\left(\frac{P_4}{P_1}\right)^2 - 1\right]h_o^2 x(2B + \alpha x)}{2(R_o - R_i)h_m(B + \alpha x)^2}\right)^{1/2} \tag{3}$$

c. Sealing dam force

Parallel film case

$$F = \frac{2P_1 L(R_o - R_i)\left[1 - \left(\frac{P_4}{P_1}\right)^3\right]}{3\left[1 - \left(\frac{P_4}{P_1}\right)^2\right]} \tag{4}$$

Small deformation case

$$F = L\int_0^{R_o - R_i} (P - P_{min})\,dx \quad \text{(Evaluated numerically)} \tag{5}$$

Typical pressure gradients across the primary seal for two design points (idle and take-off) for the 16.76 cm (6.60 in.) diameter seal are shown in Fig. 7; these data were developed by the analytical procedures of Ref. 5 and is given in more detail in Ref. 9. The important point is that choked and nonchoked flows can have pressure gradients with very different shapes thus affecting the opening force, which is the integrated force under the pressure-gradient curves.

Self-Acting Geometry

The self-acting geometry (lift pads) consist of a series of shallow recesses, typically about 25 μm (0.001 in.) deep, arranged circumferentially around the seal under the primary seal face as shown in Figs. 4 and 5. An important point is that the lift pads are bounded at the inside diameter and the outside diameter by the sealed pressure P_1. (This is accomplished by feed slots connecting the annular groove directly under the primary seal.) Therefore, the pressure gradient, due to gas leakage, occurs only across the primary seal and not across the self-acting geometry.

The self-acting geometry is approximated by the mathematical model (shown in Fig. 8) in which the curvature effects have been neglected. This mathematical model and associated analysis are described in detail in Ref. 10; the following restrictions apply:

1. The fluid is Newtonian and viscous.
2. A laminar flow regime is assumed.
3. Body forces are negligible.

Figure 9 shows the calculated lift force (see Ref. 10 for details) produced by the self-acting geometry for idle and take-off seal conditions. Inspection of Fig. 9 reveals that at film thicknesses of 2.7 μm (0.0005 in.) and greater the lift force is small. However, at film thicknesses less than 2.7 μm (0.0005 in.) the lift force increases as the film thickness decreases, and as a result the self-acting geometry has a high film stiffness which enables the seal head to track the face runout motions of the rotating seat face. As mentioned previously, the self-acting lift force tends to open the seal, and is added to the primary seal opening force to obtain the total opening force.

Closing Forces

The closing forces acting on the primary ring are a spring force and a pneumatic force. Since the full sealed pressure acts to the inside diameter of the primary seal, the net pneumatic closing force acts only on the annular area between the primary-seal inside diameter and the secondary-seal outside diameter. For the 16.76-cm (6.60-in.) diameter seal this annular area (see Fig. 10) is 4.66 cm^2 (0.722 $in.^2$), and the resulting closing forces due to the sealed pressure are listed in Tab. I, for idle and take-off sealed pressures. It should be noted that these closing forces are for average dimensions at room temperature. At operating temperature a thermal growth difference may cause a change in the relation between the secondary-seal outside diameter and the inside diameter of the primary seal. Thus, the closing force could be a function of temperature.

Equilibrium Film Thickness

In a rubbing contact seal the closing force is resisted by solid-surface rubbing contact; thus, a total force balance is achieved. But in self-acting seals the force balance is achieved without rubbing contact. Therefore, for a given design point the seal will operate at a film thickness such that the

total opening force exactly balances the total closing force, and, as illustrated in Fig. 11 from Ref. 9, the intersection of these force curves gives the steady-state equilibrium film thickness. (This film thickness determination does not take into account dynamic running factors such as seat face runout and piston ring damping.)

Each operating point should be checked for equilibrium film thickness. If these film thicknesses are not satisfactory, it may be possible to adjust the closing force such that all operating points fall within a satisfactory limit. Experience has shown that the satisfactory film thickness regime is about 2.5 μm (0.0001 in.) on the low end (some tolerance to thermal deformation must be maintained) and 0.0013 μm (0.0005 in.) on the high end. These limits are only approximate and depend to a large extent on the dynamic and thermal condition to which the seal is subjected. The high limit of practical film thickness is established by seal dynamics and leakage considerations. In particular, the primary ring response to the seat face runout becomes excessive as the mean film thickness increases (Ref. 11); this is because the stiffness of the gas film decreases as the film thickness increases.

Performance Maps

Once the equilibrium film thickness is found, the predicted leakage can be determined by using the one-dimensional method outlined in Ref. 5. By cross-plotting the equilibrium film thickness over the leakage curves, a performance map can be generated; and typical data for the 16.76-cm (6.60-in.) diameter seal is given in Fig. 12 (from Ref. 12). Inspection of Fig. 12, which covers a range of sealed pressure differential from 34 to 276 N/cm^2 (50 to 400 psi), reveals that air leakage increases as speed is increased; this is due to more effective Reyleigh step bearing performance. Also for any given speed, as pressure is increased, the equilibrium film thickness increases slightly. This suggests that the net pneumostatic force (pressure gradient across the sealing dam minus the closing force due to the sealed pressure) is decreasing slightly.

Performance maps (Fig. 13) for a smaller seal (6.44 cm (2.54 in.) nominal diameter) are similar except that the design selection of the pneumostatic force balance led to a decreasing film thickness with increasing pressure. Figure 14 shows the construction details of a small diameter seal design.

Care is taken to insure flatness of the sealing surfaces after assembly. The seal seat is keyed to the shaft spacer and is axially clamped by a machined bellows which exerts a predetermined clamping force, thus minimizing distortion of the seal seat. The bellows also acts as a static seal between the seat and the shaft spacer. Cooling oil is passed through the seat to reduce thermal gradients, and the oil dam disc also serves as a heat shield. Windbacks are used to prevent oil from approaching the sealing surfaces.

Inlet Effects

As mentioned previously, shaft seals for gases have very small sealing gap heights h (direction perpendicular to the leakage flow), and these are in the range of 2.5 to 12.5 μm (0.0001 to 0.0005 in.). In the direction of flow the gap length ℓ is relatively long, in the range of 1270 μm (0.05 in.). In other words the leakage channel is long and narrow with ℓ/h ratios of over 100. The mathematical modeling of this leakage channel is critical, in that the validity of the equilibrium film thickness prediction depends to a large part on the accuracy of predicting the pneumostatic opening forces on the primary seal; this is the pressure gradient which accompanies the leakage flow. The fully developed portion of the flow is readily obtained (Ref. 5), but the entrance region loss data for seal configurations and operation is generally not available.

Data with some applicability has been developed for gas lubricated bearings. But the flow in the cavity region just before the inlet of gas thrust bearings is generally different from that before seal configurations because the flow to the inlet of thrust bearings is often a strong function of radius and not so for seals. For this reason the inlet condition in bearings can be sonic or even supersonic. In this regard sonic, or supersonic, inlet flow is not predicted by the seal mathematical model (Ref. 5); and subsonic inlet flows are thought to prevail.

As an illustration of inlet effects the mathematical model of Ref. 5 was used to calculate the pressure gradient for the small diameter seal depicted in Fig. 14. Assumed gap thicknesses were from 2.54 to 12.7 μm (0.0001 to 0.0005 in.) and the operating conditions assumed were

Sliding speed	198 m/sec	(650 ft/sec)
Sealed gas temperature	677 K	(750° F)
Sealed gas pressure (P_1)	148 N/cm^2 abs	(214.7 psia)
Bearing cavity pressure (P_4)	25.6 N/cm^2 abs	(37.1 psia)

A constant inlet coefficient of 0.6 was assumed for the range of gap heights, and the pressure gradient curves are as shown in Fig. 15, in which the areas under the curves represent an opening force. An important point is the inlet pressure loss: the mathematical model predicts that the smaller leakage gaps have less inlet loss than the larger gaps (assuming the inlet coefficient is constant). The other point to note is that the larger gaps are operating under choked flow conditions at the exit, while the smaller gaps are not choked. The choked flow condition tends to increase the area under the curve, but the inlet loss tends to decrease the area (decrease closing force). The net result is a smaller closing force exists under the curves for the larger gaps. This is beneficial since it introduces positive axial film stiffness; that is, if the leakage gap closes, the opening force increases, and this tends to hinder further closing. This is a desirable feature since it is a positive stabilizing force from a dynamic operating standpoint.

In order to check the inlet loss coefficient magnitude which applies to seals, experiments were made using a scaled-up simulated primary seal with a fixed clearance of 25.4 μm (0.001 in.). A schematic of the test rig is shown in Fig. 16, and an example of the data obtained is shown in Fig. 17 for a pressure ratio of 10 with an upstream reservoir pressure of 62.1 N/cm^2 (90 psia). In addition to the inlet loss the pres-

ORIGINAL PAGE IS
OF POOR QUALITY

sure gradient across the primary seal was measured by means of a set of small diameter pressure taps.

Analysis of the data shows the inlet coefficient to be 0.66. In addition the data provides a convenient check on the accuracy of the primary seal pressure gradient model of Ref. 5. Figure 17 shows some deviation between the measured data and the calculated profile but the agreement is good. It should be noted that a slight convergent deformation, if it actually exists in the rig, will produce the deviation shown. And, in fact, analysis revealed that theory and experiment will agree exactly if a convergent deformation of 0.0004 radian is assumed; and for this case the coefficient drops to 0.61. It is apparent from theoretical data (Fig. 15) and measured data (Fig. 17) that neglect of inlet effect in the mathematical model for the pressure gradient will result in a predicted opening force which is too large. This is the significant point of the data.

Adverse Operating Conditions

Effect of nonparallel sealing faces. - Figure 18 shows, in an exaggerated manner, the axisymmetric coning displacement of the seal seat. (The primary ring could also be coned.) This type of coning displacement, which can be caused by thermal gradients, results in nonparallel faces within the primary seal and the self-acting geometry. These nonparallel faces have a significant effect on load capacity of the self-acting geometry; also the primary seal opening force is affected. Thus, in design, the equilibrium operating film thickness should also be calculated for anticipated coning displacements.

As an example of the effect of this coning, cruise condition operation was checked (using the methods of Ref. 9) for equilibrium film thickness for a distortion of 13 μm (0.0005 in.) across the self-acting pad. This is a distortion of 2 milliradians and is typical of some seal operation (Ref. 12).

Figure 19 shows the self-acting lift force for the 2-milliradian distortion of the seat face. Note that the force is plotted as a function of the mean film thickness of the self-acting pad. Also plotted is force generated for a parallel film, and comparison shows a significant reduction in lift force due to the axisymmetric coning, especially at the lower film thicknesses.

As noted previously, the primary seal opening force is also affected by nonparallel faces; and this was calculated by using an analysis similar to Ref. 7 for the 2-milliradian distortion. The results are given in Fig. 20. For the divergent deformation shown in Fig. 18, there is a marked reduction in opening force as the film thickness decreases (negative film stiffness). In contrast, for convergent deformation the opening force increases as film thickness decreases (positive film stiffness). However, in aircraft mainshaft seals, the divergent deformation is a natural tendency due to thermal gradients.

Finally, in Fig. 21 the equilibrium film thickness for a 2 milliradian distortion is found by finding the intersection between the total closing force and total opening force. The mean film thickness is about 1.69 μm (0.00066 in.). Thus the minimum film thickness is 10.4 μm (0.00041 in.).

With the equilibrium film thickness values for the axisymmetric distortion, the gas leakage was calculated by using the method previously outlined. The results revealed that the leakage rate for the 2-milliradian deformation was nearly twice that of the parallel-face case.

Effect of seat face runout. - The preceding analyses were for operating film thicknesses that did not vary with time. This would be the situation if the rotating seat face had zero runout. However, the seat face will, in general, have some runout with respect to the seat's axis of rotation; and in particular, the maximum runout used in practice is of interest since it will induce the maximum time-dependent film thickness changes.

Of interest, then, is how the primary ring responds to the runout motions of the seat face. This response determines the film thicknesses at any instant. Experimental data reported in Ref. 13 reveal that the primary ring can follow (dynamically track) the seat face motion over a considerable range of face runouts. These data were obtained by mounting two proximity probes (90° apart) on the ring retainer and recording the change in film thickness as a function of time. A schematic showing the probe location is given in Fig. 22. Some results from Ref. 13 are given in Fig. 23 which shows that for a seat face runout of 20 μm (0.00085 in.) full-indicator reading (F.I.R.), the ring response is in phase and the total change in film thickness is 17 μm (0.00067 in.) and that the film thickness varies circumferentially; that is, the film thickness is not axisymmetric and is similar to that depicted in Fig. 24.

This nonsymmetric angular misalignment is an inherent tendency because of secondary seal friction and seal head inertia, which are introduced by the tracking response to the seat face axial runout. As the high point of the seat face runout (see Fig. 24) rotates, the seal head must move back, and this is resisted by the secondary seal friction and head inertia; thus the film thickness tends to be smaller opposite the high point of face runout. In contrast, the friction and inertia are acting in opposite directions at the low point (180° away). Therefore, a rotating force couple exists which is synchronous with the face runout (if the seal head is properly tracking the seat motion); this causes the sealing faces to have an inherent angular misalignment.

As previously indicated, nonparallel faces cause changes in the pressure gradient across the primary seal and, therefore, effect the contribution of the primary seal to seal stability; this contribution can either have a positive (converging faces) or negative (diverging faces) effect. Table II (from Ref. 14) outlines some of the possible primary seal distortions, axisymmetric and nonaxisymmetric; and the resultant contribution for seal stability is indicated. Table II was constructed for incompressible fluid but these stability models, in general, also apply when sealing a compressible gas. For gas turbine mainshaft seals, model E, with the sealed pressure at the inside diameter, is probably the most prevalent with the nonaxisymmetric displacement (angular misalignment) being produced by the response of the seal head to the face runout motions of the seat. The axisymmetric portion of the nonparallel displacement will be due to thermal gradient which arises because of two effects: (a) the temperature gradient between the sealed gas and the bearing sump, and (b) the shearing of the fluid film in the primary seal. Analysis suggests that

the thermal coning can readily predominate, therefore, with reference to model E of Tabl II, β will be greater than γ, and the seal force will be divergent over the full 360°; this is a destabilizing condition, and overall seal stability must be provided by the self-acting geometry if rubbing contact is to be avoided.

An analytical program has been developed for the purpose of predicting primary seal ring response to seat face runout (Ref. 11). Analysis of the 16.67-cm (6.60-in.) diameter seal depicted in Fig. 4 revealed that the primary ring response is markedly affected by secondary seal friction and by inertia of the primary ring assembly. The friction effect is illustrated in Fig. 25; as runout increases, there is a friction level that, if exceeded, will retard the primary ring motion to such an extent that rubbing contact will occur (line (1)); also for the higher face runouts there is a friction level below which the inertial forces are so high that the primary ring cannot follow the runout (line (2)). Therefore, some friction is probably desirable for most applications because of the practical limits on control of face runouts. Further, the data suggest that the primary ring assembly inertia should be kept as small as practical in order to maintain good response (avoid unstable operation).

In a detailed analysis (Ref. 11) three different types of nosepiece responses were revealed by a parametric study using different magnitudes of seat face runout and secondary seal friction. These three cases are

Case 1 - Primary ring motion duplicates seat face runout motion and can be described by rotation (rocking) about two orthogonal axes. However, because of primary ring inertia and/or friction, the face of the ring has an angular misalignment with respect to the face of the seat. Therefore, the film thickness between the faces is not uniform (see Tab. II, model D).

Case 2 - Same as case 1 plus an additional axial vibration component.

Case 3 - Seal failure (film thickness reaches zero). This case can occur when the frictional forces are either two low (when inertia forces are high) or too high for the available load capacity of the self-acting pads.

An analysis was made of the seal head dynamic response of the 6.44-cm (2.54 in.) diameter seal with a seat face runout of 13 μm (0.000512 in.) and with secondary seal friction considered. The mathematical model described in Ref. 11 was used, and the data are given in Fig. 26, in which the minimum film thickness is given as a function of time for a seal sliding speed of 244 m/sec (800 ft/sec). The plot in Fig. 26 shows stable operation with a minimum film thickness of 5.6 μm (0.000219 in.) was achieved within a very short time span; stable operation of the case 1 type (tracking without axial vibration) was predicted.

EXPERIMENTAL DATA

16.76-Centimeter (6.60-In.) Nominal Diameter Seal

Table III (from Ref. 12) shows typical experimental data on the large diameter seal. The maximum combined conditions attempted in the rig test were a sliding speed of 175 m/sec (575 ft/sec), a sealed gas temperature of 811 K (1000° F), and a sealed pressure of 207 N/cm^2 gage (300 psig). This set of data and resulting posttest inspection of the parts confirmed the analytical predictions that the seal would function without rubbing contact at operating conditions expected in advanced engines.

Figure 27 (from Ref. 12) shows some experimentally obtained leakage results compared with the predicted total leakage (combined primary and secondary seal leakage). The correlation is reasonable, and the experimental data show the scatter typical of leakage values obtained throughout the test. This scatter in results is due to the strong dependence of leakage on sealing clearance (A very small change in clearance will produce a significant change in leakage. See formula (1).)

In addition to the performance evaluation at various operating conditions, the seal was subjected to a 320-hour endurance test (Ref. 15) at the following test conditions:

	120-hr segment	200-hr segment
Sealed air temperature	775 K (1000° F)	775 K (1000° F)
Sealed pressure differential	138 N/cm^2 (200 psi)	138 N/cm^2 (200 psi)
Seal velocity	122 m/sec (400 ft/sec)	122 m/sec (400 ft/sec)
Spring load	68.5 N (15.4 lb)	68.5 N (15.4 lb)

During the first segment of testing, seal leakage averaged approximately 0.33 scmm (11.7 scfm) as shown in Fig. 28. During the second segment, leakage averaged 0.40 scmm (14 scfm) for the first 100 hours, and increased at the rate of approximately 0.03 scmm (1 scfm) every 20 hours for the second 100 hours.

Inspection of the seal after the 320 hours suggested that the gradual increase in leakage was due to air-entrained debris erosion of the sealing dam. (Erosion due to debris is discussed in the following section.) A profile trace of the carbon primary seal face taken after 120 hours of endurance is shown in Fig. 29(a). The deepest scratch (air entrained debris) in the sealing dam was approximately 5.08 μm (0.0002 in.). The average Rayleigh pad wear for the 120-hour test was less than 1.27 μm (0.00005 in.).

After the second segment of testing the carbon primary seal and seal seat were still in good condition. A profile trace (Fig. 29(b)) taken at the same location as the traces in Fig. 29(a) shows more shallow scratches 2.54 μm (0.0001 in.) deep. The average wear on the Rayleigh pads for the second segment of 200 hours was less than 1.27 μm (0.00005 in.).

The effects produced by air entrained debris were checked by the introduction of abrasive particles

ORIGINAL PAGE IS
OF POOR QUALITY

(Arizona road dust) into the test rig at the rate of 3.5 g/hr over a 14.5-hour test run. Data indicated a gradual increase in seal leakage due to wear of the sealing dam by the air entrained dirt. No significant wear occurred to the Rayleigh step pad portion. The erosion wear pattern of the primary seal is shown in Fig. 30, which is a surface profile trace taken radially across the primary seal. It is thought that the sealing dam wear may proceed until the leakage gap height becomes large enough to pass the entrained debris.

6.44-Centimeter (2.54-In.) Nominal Diameter Seal

Table IV contains gas leakage data for relatively small diameter self-acting seals (see Fig. 14) operating in a test rig over a pressure differential range from 23 to 111 N/cm^2 (34 to 161 psi) and a sliding speed range from 91 to 183 m/sec (300 to 600 ft/sec). (This is a rotative speed range of 27 300 to 54 600 rpm.)

The test setup contained two seals, one fore and one aft of the rig bearing. This simulated a bearing compartment in a small gas turbine. Neither the forward nor the aft carbon nose or seal seat showed any wear during this evaluation (Tab. IV, from Ref. 16). Thus the sealing surfaces were separated by a gas film over the entire matrix of operating variables. This suggests that the gas bearing film stiffness was sufficient to prevent rubbing contact under the high inertia forces which are associated with high rotative speeds (inertia forces increase as the square of the rotating speed).

Data in Tab. IV indicate a seal leakage increase with a sliding speed increase (for any given pressure differential). This leakage increase is due to a slight increase of the sealing gap.

To further explore the operating limits of the small diameter self-acting seals, 500 hours of endurance operation at ambient temperature (~381 K (225° F)) was conducted as follows (Ref. 16):

Hours	Speed			Air pressure differential (max)	
	m/s	ft/sec	rpm	N/cm^2 abs	psia
1 - 100	145	475	43 000	125	181
100 - 200	152	500	45 500	129	186.5
200 - 300	160	525	47 700	130	189
300 - 400	168	550	50 000	129	187
400 - 467	175	575	52 300	128	186
467 - 500	183	600	54 600	128	186

The same aft seal carbon and seat were used throughout the test, and a forward carbon ring was used that had previously operated for 150 hours.

Table V from Ref. 16 outlines test results for the 500-hour run. The last run was typical of the airflow that can be expected through two seals at an air pressure differential of 127 N/cm^2 (184 psi); approximately 0.007 kg/sec (12 scfm or 0.015 lb/sec).

The depth of the self-acting geometry was checked by surface profile measurements for the purpose of monitoring the wear process. The average total wear of the carbon rings during the 500-hour test was 51 μm (0.0002 in.) (Ref. 16). In addition to endurance runs, the effect of seat face runout was evaluated in a 10-hour test run by using seats which had been machined such that in the assembled state a full indicated runout of 50.8 μm (0.002 in.) existed; this magnitude is twice the usual practice for conventional seals of this size range. Baseline tests were also conducted on seal assemblies which had runouts of 15 μm (0.0006 in.). A comparison of leakage rates is shown in Fig. 36. Maximum speed was 43 000 rpm or 145 m/sec (475 ft/sec). The data of Fig. 31 reveal a significant axial runout effect on leakage rate, the seals with 50.8-μm (0.002-in.) seat face runout - having about three times the leakage of the seals with normal runout values (15 μm (0.0006 in.)). Inspections after the two tests, 10 hours of baseline testing and 10 hours of testing with 40.8-μm (0.0020-in.) runout, revealed that wear was insignificant; therefore, noncontact operation was maintained in both 10-hour tests. The increase in leakage over the baseline test is due to a greater average film thickness induced by response of the primary ring to the seat face runout (see previous discussion on effects of seat face runout).

Spiral Groove Self-Acting Seal

The Rayleigh step bearings of the small diameter seal depicted in Fig. 14 were replaced with a set of spiral grooves (see Fig. 32), and the seal was run at simulate engine conditions. Typical seal leakage data are shown in Fig. 33 (from Ref. 17) for sliding speeds of 182.9 m/sec (600 ft/sec). Data at other sliding speeds confirmed that the general trend for self-acting seals was a leakage increase as speed increased. The leakage, however, was relatively low and considered within the usable range for application in small gas turbine engines.

A 54-hour endurance run was made at 148.1 N/cm^2 abs (215 psia) sealed pressure and the data are given in Tab. VI. The sliding speeds ranged from 122 to 243.8 m/sec (400 to 800 ft/sec), with the majority of the time being at 213 m/sec (700 ft/sec). The maximum sliding speed of 243.8 m/sec (800 ft/sec) corresponds to a maximum rotating speed of 72 500 rpm.

The measured wear in the spiral groove region after the 54 hours of operation was (Ref. 17):

Forward seal. . . . . No measurable wear
Aft seal. . . . . 1.0 μm (0.000040 in.)

Leakage Rate Comparison to Conventional Seal

Leakage tests were made on various conventional seals of a size comparable to the 6.44-cm (2.54-in.) diameter Reyleigh step pad seal (Fig. 14); the comparison is shown in Fig. 34. In general, the plot shows that the self-acting face seal has the potential of significantly reducing leakage as compared with the conventional seals.

Of the conventional configurations, face seals allowed the least air flow at high pressure differentials. Circumferential segmented seals are as tight as face seals at moderate operating conditions; however, experience and the subject test program results have shown that at pressure differentials above 41.4 N/cm^2 (60 psi) and speeds above 107 m/sec (350 ft/sec), these (unbalanced) circumferential segmented seals rapidly wear out and finally operate as labyrinths. In that case there is little to choose between circumferential, rotating ring, and labyrinth seals in terms of air flows.

To gain some perspective of the magnitude of air flow under discussion, engine experience has shown that excessive air flow into a bearing package incorporating seals of the size used in the test program would be in the order of 0.012 kg/sec (0.029 lb/sec). Taking midpoint values of the range of pressure differentials in Fig. 34, the face seal could not meet this criterion at pressure differentials above approximately 85 N/cm^2 (123 psi), and the limiting pressure differential for circumferential segmented seals (which wear rapidly), rotating ring seals, and simple labyrinths would be approximately 40 N/cm^2 (58 psi). The self-acting seal, however, did not reach the limiting leakage rate and had a leakage of 0.0046 kg/sec (0.0102 lb/sec) at a pressure differential of 107.6 N/cm^2 (156.0 psi). In general the self-acting seal had about one third the leakage of the conventional face seal.

CONCLUDING REMARKS

Self-acting seals are described, and their potential for meeting operational requirements of gas turbine engines is explored by means of predictive analysis of their operation at sealing speed, pressure, and temperature conditions which would be imposed by the engine. In particular, the analytical procedure is given for predicting the leakage and operating film thicknesses. Performance maps for two seal sizes are given; these are a 16.76-cm (6.60-in.) nominal diameter seal suitable for large engines and a 6.44-cm (2.54-in.) diameter seal for small engines. The analysis and subsequent operation of these seals under simulated gas turbine conditions revealed the following:

1. Analysis

a. Noncontact operation with acceptable leakage is predicted over the range of engine operation conditions (idle, takeoff, climb, and cruise) for both seal sizes.

b. The predicted operating film thickness of the 16.76-cm (6.60-in.) diameter seal ranged between 4.6 and 11.9 μm (0.00018 and 0.00047 in.) for idle, takeoff, climb, and cruise.

c. The calculated seal leakage rates of the 16.76-cm (6.60-in.) diameter seal ranged between 0.01 and 0.40 scmm (0.4 and 14.0 scfm) for idle, takeoff, climb, and cruise.

d. For a typical operating condition noncontact operation was predicted under the assumption of a 2-milliradian face deformation. Gas leakage was about twice that for parallel-face operation.

e. Analysis reveals that the pressure drop in the inlet to the primary seal gives rise to a positive film stiffness and has a significant effect on seal opening force magnitude.

f. Proper tracking of the seat face runout by the carbon ring is predicted for practical levels of face runout magnitudes.

2. Experiment, Simulated Engine Operation

a. In general the self-acting seals operate, as predicted, without rubbing contact over the range of simulated engine operating conditions. Of particular interest was: (a) the noncontact operation of the 16.76-cm (6.60-in.) diameter seal at the advanced engine conditions of a 152-m/sec (500-ft/sec) sliding speed, a 345-N/cm^2 (500-psi) sealed pressure differential, and a 811 K (1000° F) sealed air temperature and (b) the noncontact operation of the 6.44-cm (2.54-in.) diameter seal at a 243.8-m/sec (800-ft/sec) sliding speed and a 148.1-N/cm^2 (215 psi) sealed pressure level.

b. The self-acting face seal leakage was significantly lower than that of conventional seal types.

REFERENCES

1. Schweiger, F. A., "The Performance of Jet Engine Contact Seals," Lubr. Eng., vol. 19, no. 6, June 1963, pp. 232-238.
2. Parks, A. J., McKibbin, R. H., Ng, C. C. W., and Slayton, R. M., Pratt & Whitney Aircraft, "Development of Main-Shaft Seals for Advanced Air Breathing Propulsion Systems," 1967, PWA-3161, NASA CR-72338.
3. Povinelli, V. P., and McKibbin, A. H., Pratt & Whitney Aircraft, "Development of Mainshaft Seals for Advanced Air Breathing Propulsion Systems," 1967, PWA-3161, NASA CR-72737.
4. Brown, P. F., Jr., "A Glossary of Seals Terms," Special Publication SP-1, American Society of Lubrication Engineers, 1969.

ORIGINAL PAGE IS
OF POOR QUALITY

5. Zuk, J., Ludwig, L. P., and Johnson, R. L , Lewis Research Center, "Quasi-One-Dimensional Compressible Flow Across Face Seals and Narrow Slots. I - Analysis," 1972, NASA TN D-6668.
6. Zuk, J., and Ludwig, L. P., Lewis Research Center, "Investigation of Isothermal, Compressible Flow Across a Rotating Sealing Dam. I - Analysis," 1969, NASA TN D-5344.
7. Zuk, J., and Smith, P. J., Lewis Research Center, "Computer Program for Viscous Isothermal Compressible Flow Across a Sealing Dam with Small Tilt Angle," 1969, NASA TN D-5373.
8. Johnson, R. L., and Ludwig, L. P., Lewis Research Center, "Shaft Face Seal with Self-Acting Lift Augmentation for Advanced Gas Turbine Engines, 1969, NASA TN D-5170.
9. Ludwig, L. P., Zuk, J., and Johnson, R. L., Lewis Research Center, "Design Study of Shaft Face Seal with Self-Acting Lift Augmentation. IV - Force Balance," 1972, NASA TN D-6368.
10. Zuk, J., Ludwig, L. P., and Johnson, R. L., Lewis Research Center, "Design Study of Shaft Face Seal with Self-Acting Lift Augmentation. I - Self-Acting Pad Geometry," 1970, NASA TN D-5744.
11. Colsher, R., and Shapiro, W., Franklin Research Institute, "Steady State and Dynamic Performance of Gas-Lubricated Seals, 1972, F-C3452-1, NASA CR-121093.
12. Dobek, L. J., Pratt & Whitney Aircraft, "Development of Mainshaft Seals for Advanced Air Breathing Propulsion Systems," 1973, PWA-TM-4683, NASA CR-121177.
13. Hady, W. F., and Ludwig, L. P., Lewis Research Center, "Experimental Investigation of Self-Acting-Lift-Pad Characteristics for Main Shaft Seal Applications." 1971. NASA TN D-6384.
14. Ludwig, L. P., Lewis Research Center, and Greiner, H. F., Sealol Inc., "Design Considerations in Mechanical Face Seals for Improved Performance - II Lubrication," NASA TM X-73736, 1977.
15. Povinelli, V. P., and McKibbin, A. H., Pratt & Whitney Aircraft, "Development of Mainshaft Seals for Advanced Air Breathing Propulsion Systems, Phase II," 1970, PWA-3933, NASA CR-72737.
16. Lynwander, P., Avco Lycoming Division, "Development of Self-Acting Seals for Helicopter Engines," 1974, LYC-74-55, NASA CR-134739.
17. O'Brien, M., Avco, "Development of Spiral Groove Self-Acting Face Seals," 1977, LYC-77-41, NASA CR-135303.

E-9446

TABLE I. - CLOSING FORCE

	Design point	
	Idle	Takeoff
Sealed gas temperature.	311 K (100° F)	977 K (1300° F)
Seal sliding speed.	122 m/sec (200 ft/sec)	137 m/sec (450 ft/sec)
Sealed pressure, P_1	45 N/cm^2 a (65 psia)	217 N/cm^2 a (316 psia)
Pressure change, ΔP	34.5 N/cm^2 (50 psi)	207 N/cm^2 (300 psi)
Sealed-pressure closing force, F_p	160.6 N (36.1 lbf)	963.4 N (216.6 lbf)
Spring force, F_s.	71.2 N (16 lbf)	71.2 N (16 lbf)
Total closing force, $F_t = F_p + F_s$	231.7 N (52.1 lbf)	1034.6 N (232.6 lbf)

ORIGINAL PAGE IS
OF POOR QUALITY

TABLE II. - SEAL STABILITY MODELS

		Pressure pattern	Axial stiffness	Restoring moment
A. Parallel	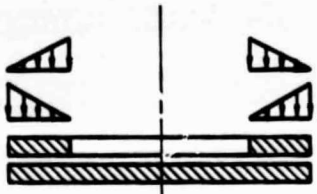			
	$P_0 < P_i$	Axisymmetric	Zero	Zero
	$P_0 > P_i$	Axisymmetric	Zero	Zero
B. Coned	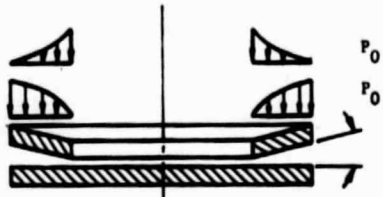			
	$P_0 < P_i$	Axisymmetric	Negative	Negative
	$P_0 > P_i$	Axisymmetric	Positive	Positive
C. Coned				
	$P_0 < P_i$	Axisymmetric	Positive	Positive
	$P_0 > P_i$	Axisymmetric	Negative	Negative
D. Misaligned	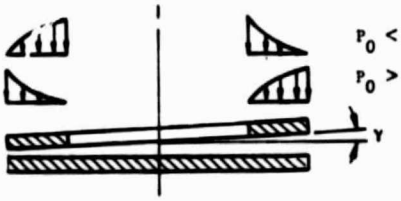			
	$P_0 < P_i$	Nonaxisymmetric	Positive	Positive
	$P_0 > P_i$	Nonaxisymmetric	Negative	Negative
E. Coned and misaligned				
	$P_0 < P_i$	Nonaxisymmetric	Negative	Negative
	$P_0 > P_i$	Nonaxisymmetric	Positive	Positive
F. Coned and misaligned	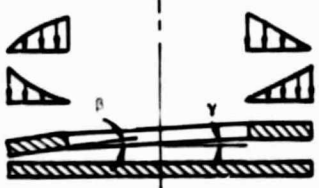			
	$P_0 < P_i$	Nonaxisymmetric	Positive	Positive
	$P_0 > P_i$	Nonaxisymmetric	Negative	Negative

ORIGINAL PAGE IS
OF POOR QUALITY

TABLE III. - TYPICAL TEST DATA FOR 16.76-CENTIMETER (6.60-IN.) NOMINAL DIAMETER SEAL[a]

Time, hr	Sliding speed		Seal pressure		Air temperature		Oil-in temperature		Actual total air leakage	
	m/sec	ft/sec	N/cm^2	psi	K	°F	K	°F	$scms \times 10^3$	scfm
2.0	111	365	207	300	700	800	394	250	15.0	31.9
2.0	↓	↓	224	325	↓	↓	↓	↓	16.5	34.9
2.0	↓	↓	241	350	↓	↓	↓	↓	17.8	37.8
2.0	↓	↓	259	375	↓	↓	↓	↓	18.8	39.9
2.0	↓	↓	275	400	↓	↓	↓	↓	19.6	41.5
2.0	122	400	275	400	↓	↓	↓	↓	26.6	56.4
8.0	122	400	293	425	↓	↓	↓	↓	27.8	59.0
1.0	137	450	207	300	↑ .1	1000	↓	↓	17.2	36.5
.5	152	500	↓	↓	↓	↓	↓	↓	17.5	37.0
.5	160	525	↓	↓	↓	↓	↓	↓	16.5	35.0
.75	168	550	↓	↓	↓	↓	↓	↓	16.5	35.0
.25	175	575	↓	↓	↓	↓	↓	↓	17.9	38.0

[a]Ref. 12.

TABLE IV. - SELF-ACTING FACE SEAL EVALUATION

[6.44-cm (2.54-in.) nominal diameter seal.]

Rpm	Speed		Air pressure differential		Airflow (two seals)		Seal temperature	
	m/sec	ft/sec	N/cm^2	psi	kg/sec	lb/sec	K	°F
27 300	91	300	23.4	34.0	<0.0006	<0.0013	333	140
36 400	122	400	23.1	33.5	<.0006	<.0013	352	174
45 500	152	500	23.1	33.5	<.0006	<.0013	371	210
54 500	183	600	22.1	32.0	.0011	.0024	392	246
27 300	91	300	111.4	161.5	.0023	.0050	364	196
36 400	122	400	110.7	160.5	.0032	.0070	373	212
45 500	152	500	109.6	159.0	.0036	.0079	386	236
54 600	183	600	107.6	156.0	.0046	.0102	402	263

E-9446

TABLE V. - 500-HOUR ENDURANCE TEST RESULTS[a]

[Sealed pressure, 148 N/cm^2 abs (215 psia).]

Hours	Maximum airflow (two seals)			Maximum cavity pressure		Maximum seal temperature				Number of stops
						Forward		Aft		
	kg/s	scfm	lb/sec	N/cm^2 abs	psia	K	°F	K	°F	
[b]1 - 100	0.011	18.5	0.024	25.3	36.7	407	272	380	225	8
[b]100 - 200	.008	13.5	.017	21.8	31.7	417	290	385	234	9
[b]200 - 300	.007	12.5	.016	21.5	31.2	421	298	390	242	21
[b]300 - 400	.008	14.5	.018	22.5	32.7	420	296	395	251	9
400 - 467	.007	12.5	.016	21.2	30.7	420	296	399	258	8
467 - 500	.007	12.0	.015	21.2	30.7	426	306	407	272	3

[a]Ref. 16.

[b]Air leakage results includes leakage through scavenge fittings.

ORIGINAL PAGE IS
OF POOR QUALITY

TABLE VI. - ENDURANCE TEST FOR 6.44-CENTIMETER (2.54-IN.) DIAMETER SPIRAL SELF-ACTING SEAL

[Sealed air pressure, 148 N/cm^2 abs (215 psia).]

Accumulated time, hr	Speed			Cavity pressure		Airflow			Seal temperature			
	m/sec	ft/sec	rpm	N/cm^2 abs	psia	kg/sec	scfm	lb/sec	Forward		Aft	
									K	°F	K	°F
4	122.0	400	35 900	28.7	41.7	0.0116	20.0	0.0255	359	188	360	189
9	152.0	500	45 100	32.0	46.7	.0119	20.5	.0261	377	220	386	235
19	183.0	600	54 100	28.9	40.7	.0093	16.9	.0204	402	263	407	273
24	213.0	700	62 900	28.1	40.7	.0079	13.5	.0172	454	358	469	385
45	213.0	700	62 900	26.7	38.7	.0070	12.0	.0153	480	405	504	448
52	215.5	707	63 800	32.2	46.7	.0104	18.0	.0229	527	490	544	520
53.7	230.7	757	68 300	34.2	49.7	.0115	20.0	.0255	547	524	559	547
54	236.8	777	70 100	34.9	50.7	.0115	20.0	.0255	550	530	563	554
54.1	243.8	800	72 500	34.2	49.7	.0115	20.0	.0255	555	540	562	553

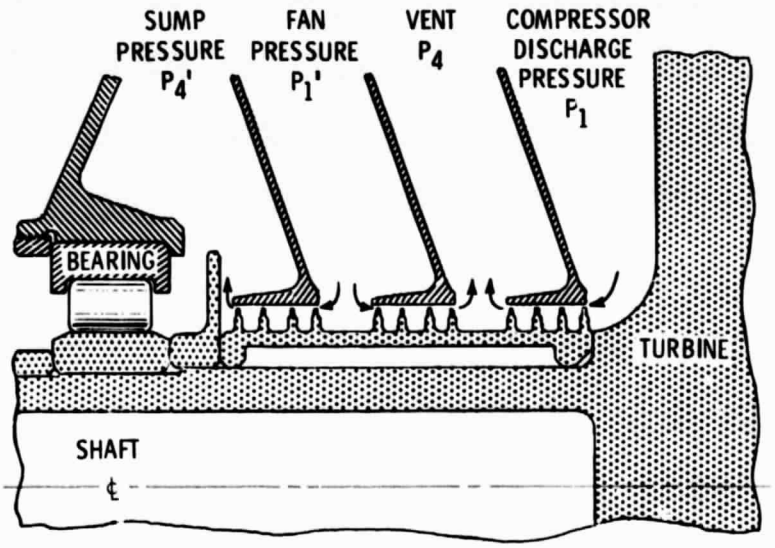

Figure 1. - Labyrinth seal system schematic.

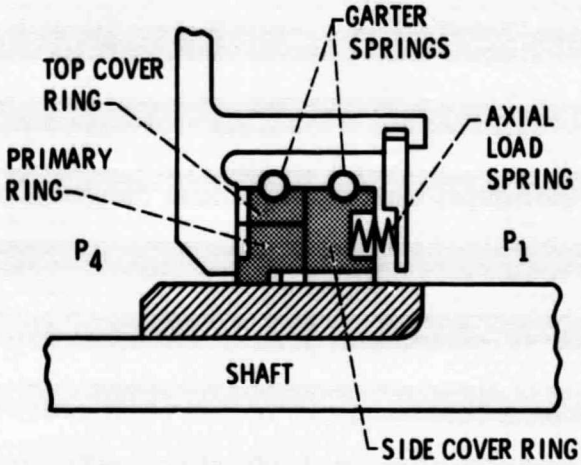

Figure 2. - Shaft riding or circumferential seal.

E-9446

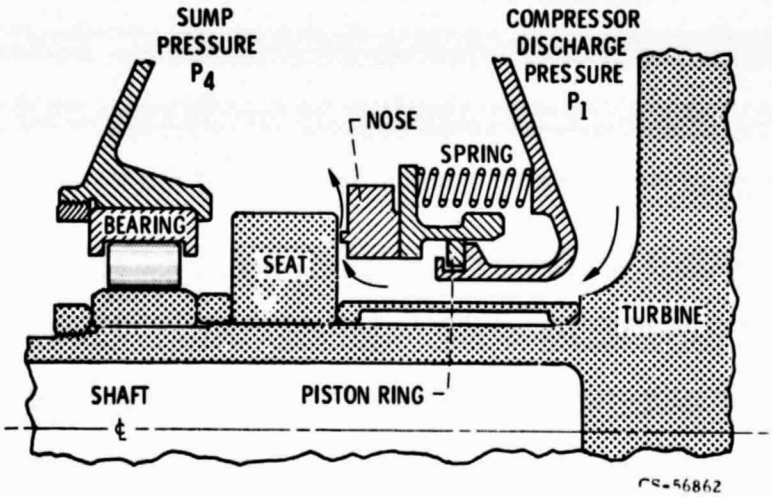

Figure 3. - Schematic of a conventional radial face seal.

ORIGINAL PAGE IS
OF POOR QUALITY

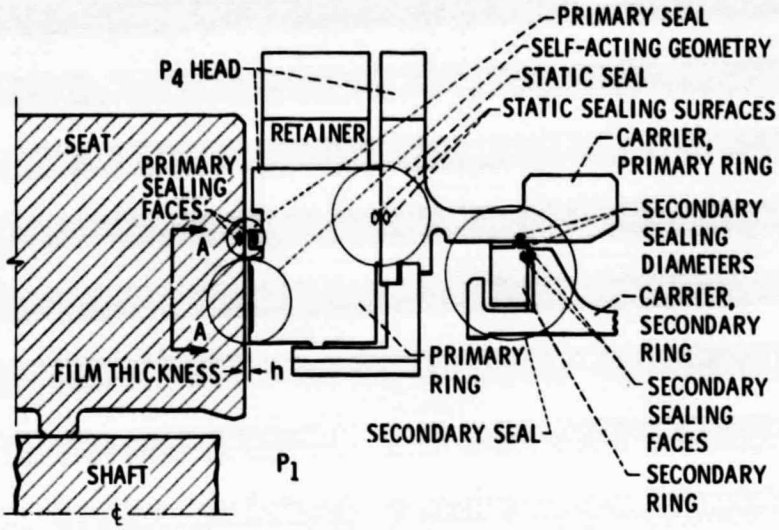

(a) NOMENCLATURE

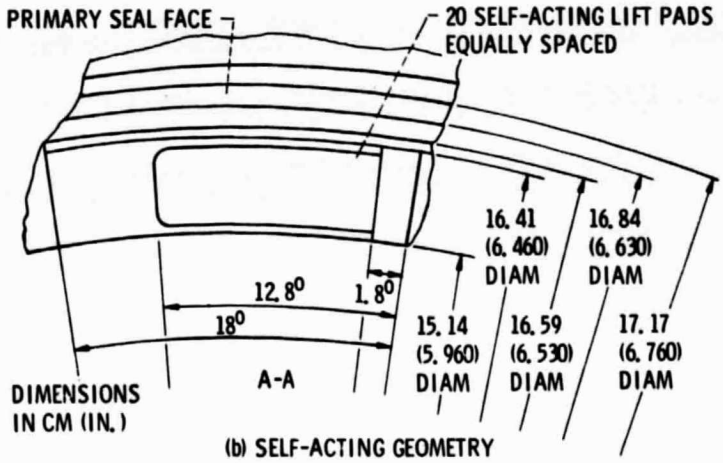

(b) SELF-ACTING GEOMETRY

Figure 4. - Self-acting face seal.

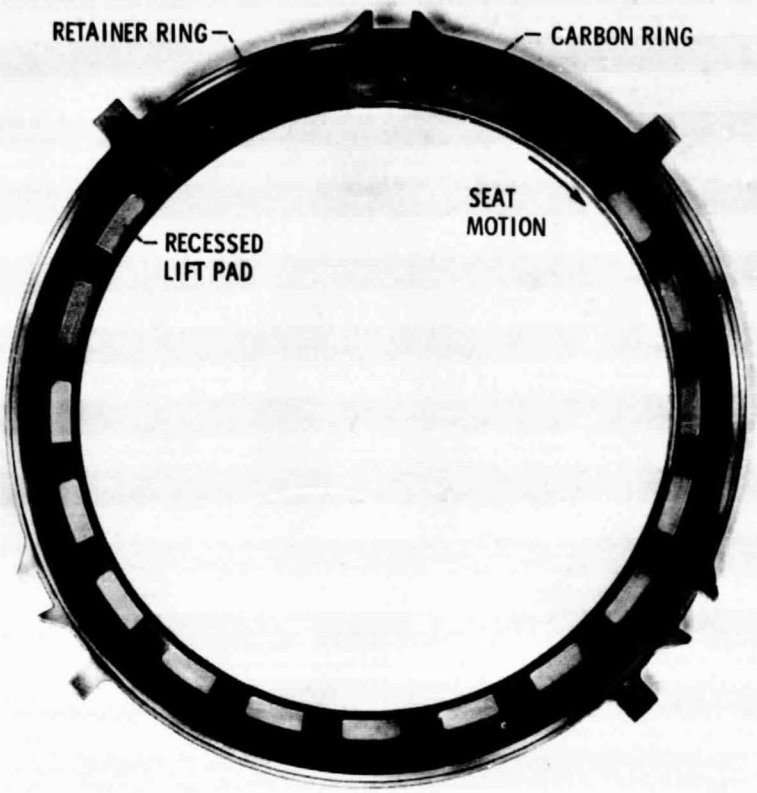

Figure 5. - Primary ring assembly.

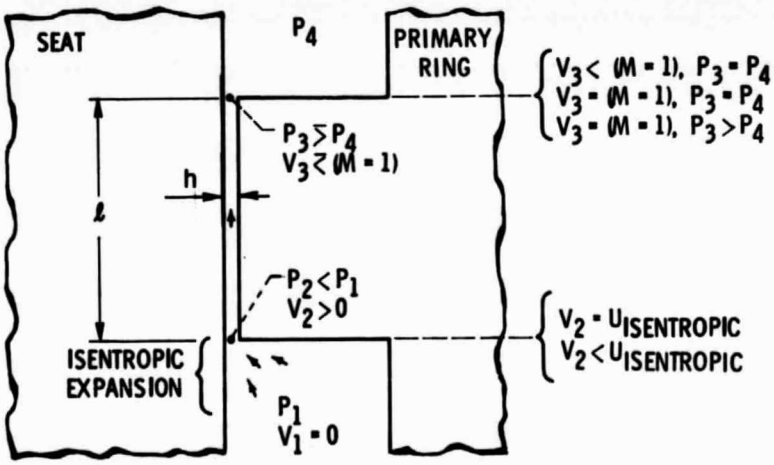

Figure 6. - Mathematical model of primary seal.

E-9446

ORIGINAL PAGE IS
OF POOR QUALITY

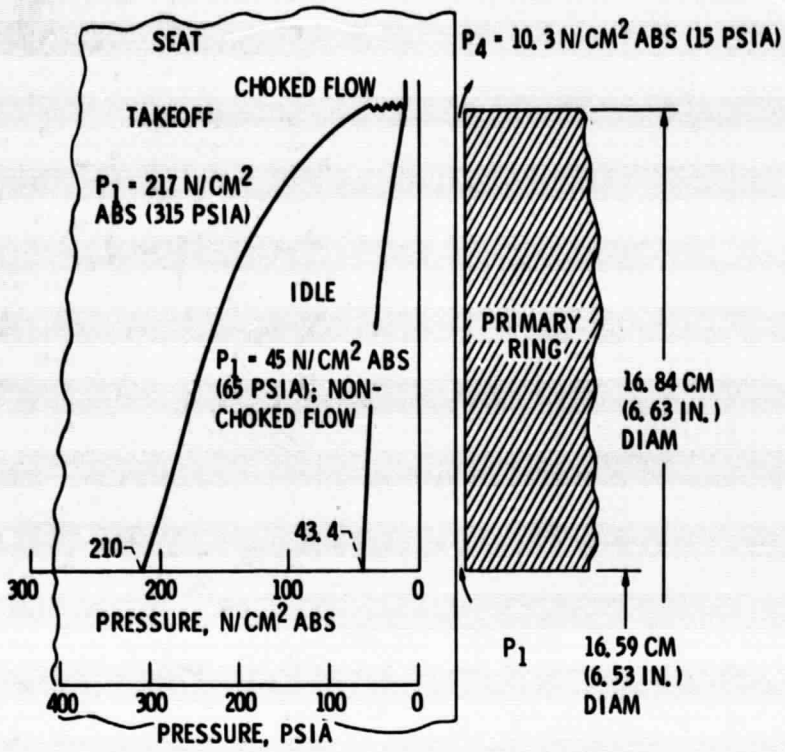

Figure 7. - Pressure gradient in primary seal, illustrating choked and nonchoked flow. Parallel faces; mean film thickness h_m, 0.0010 centimeter (0.0004 in.). (From ref. 9.)

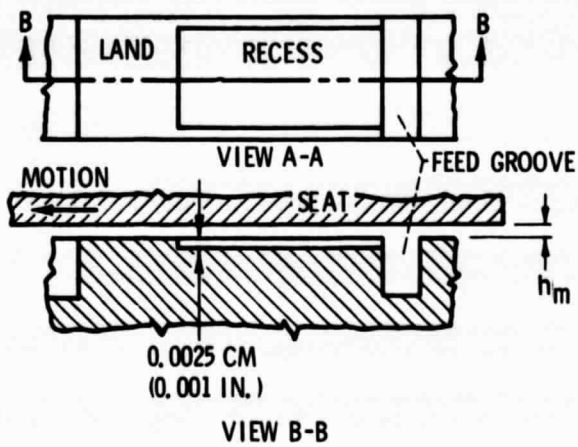

Figure 8. - Mathematical model of self-acting pad with curvature effects neglected.

E-9446

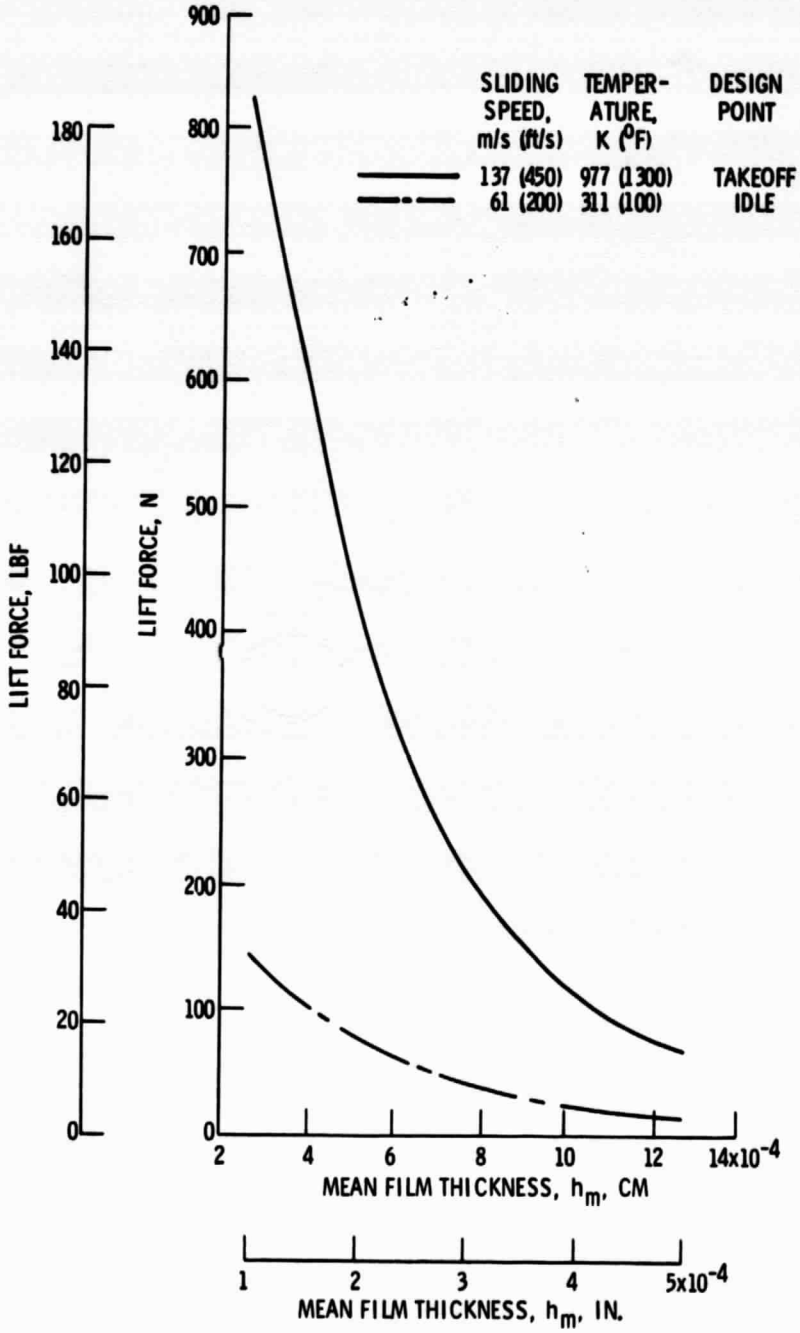

Figure 9. - Lift force of self-acting geometry, Number of pads, 20; recess depth, 0.0025 centimeter (0.001 in.); fluid, air; parallel faces. (From ref. 9.)

ORIGINAL PAGE IS
OF POOR QUALITY

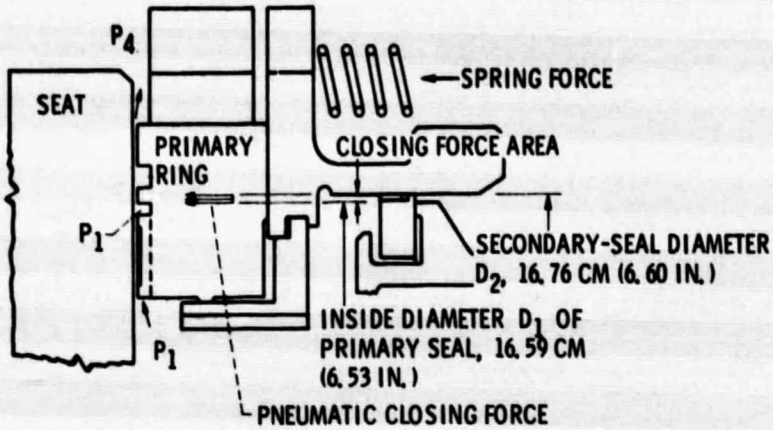

Figure 10. - Closing forces - spring force and net closing force due to sealed pressure.

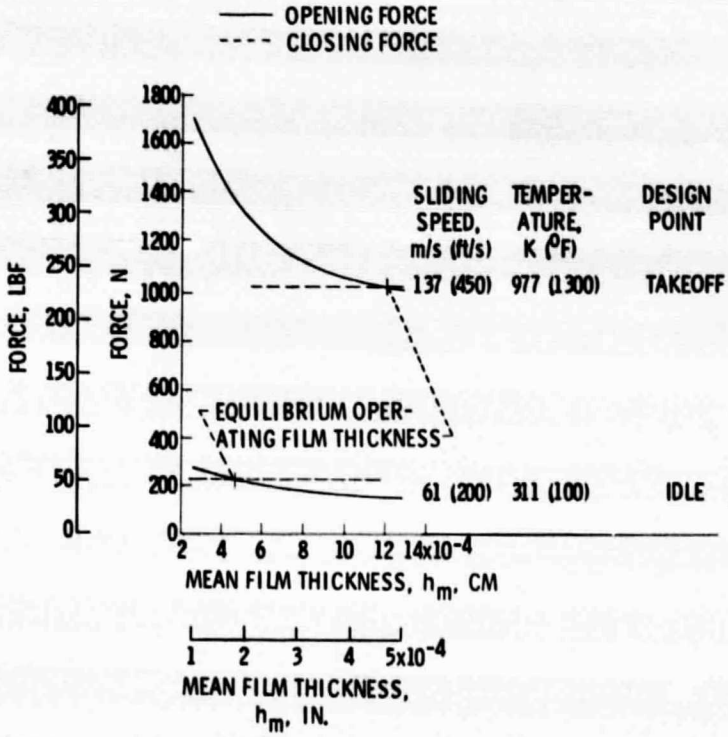

Figure 11. - Equilibrium gas film thickness as determined by total seal opening and closing forces. Parallel faces (from ref. 9).

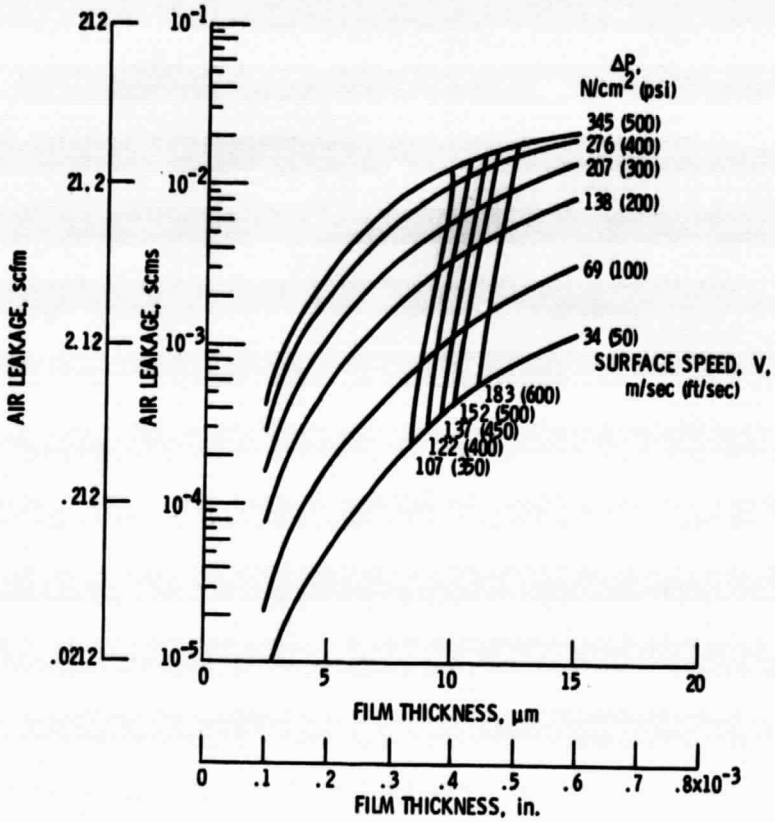

Figure 12. - Primary seal leakage as function of film thickness. Nominal diameter seal (from ref. 12), 16.76 cm (6.60 in.); seal air temperature, 700 K (800° F); spring force, 75 N (17 lbf).

E-9446

ORIGINAL PAGE IS
OF POOR QUALITY

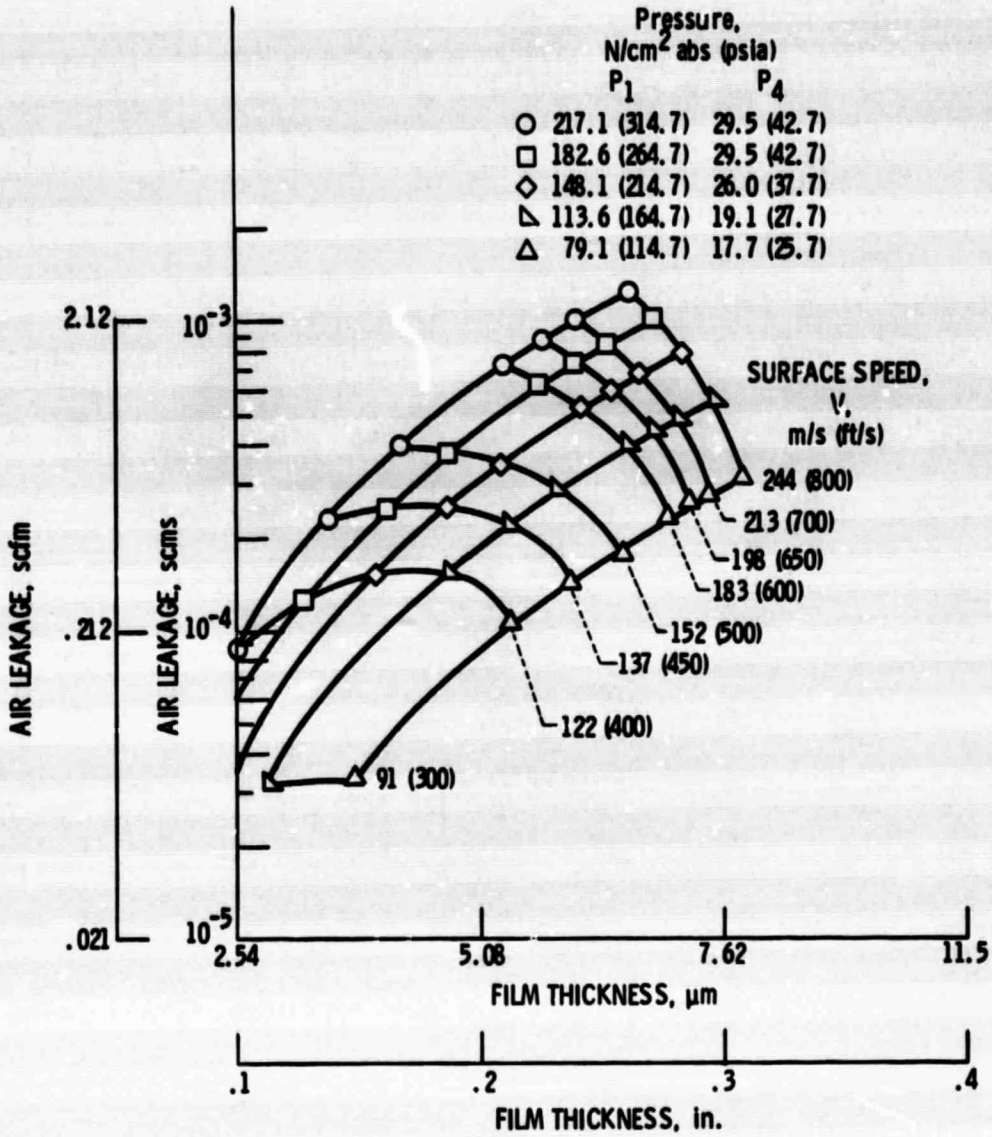

Figure 13. - Performance map for 6.44 cm (2.5 in.) nominal diameter seal. Sealed air temperature, 644 K (700° F); spring force, 31.1 N (7 lbf); inlet loss coefficient, 1.0.

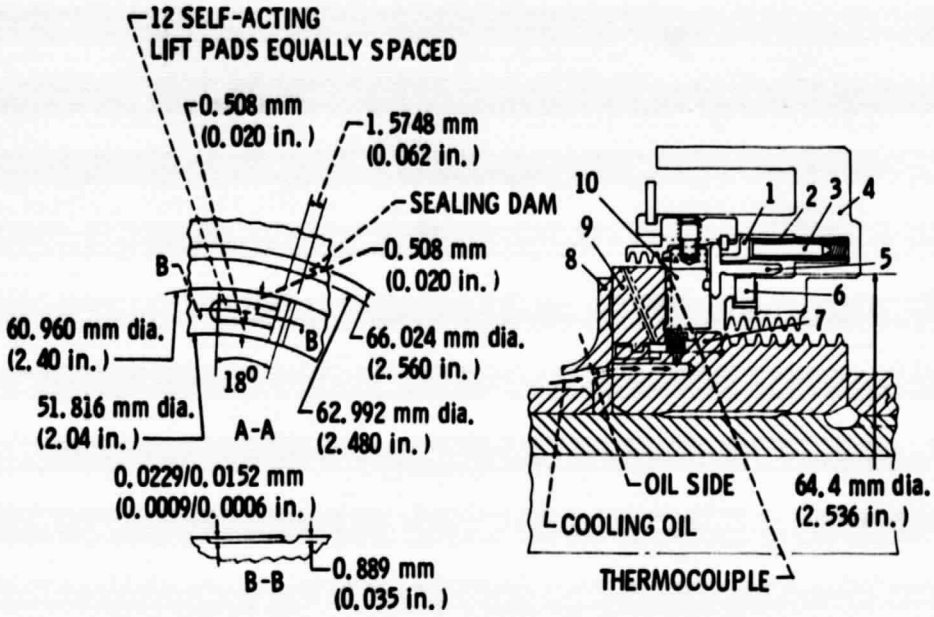

1. SPRING PLATE
2. COMPRESSION SPRING
3. SPRING PIN
4. HOUSING
5. CARRIER
6. PISTON RING (SECONDARY SEAL)
7. BELLOWS SPACER
8. OIL DAM AND HEAT SHIELD
9. ROTATING SEAT
10. NOSEPIECE

Figure 14. - Self-acting face seal design, 6.44 cm (2.54 in.) nominal diameter.

E-3446

ORIGINAL PAGE IS
OF POOR QUALITY

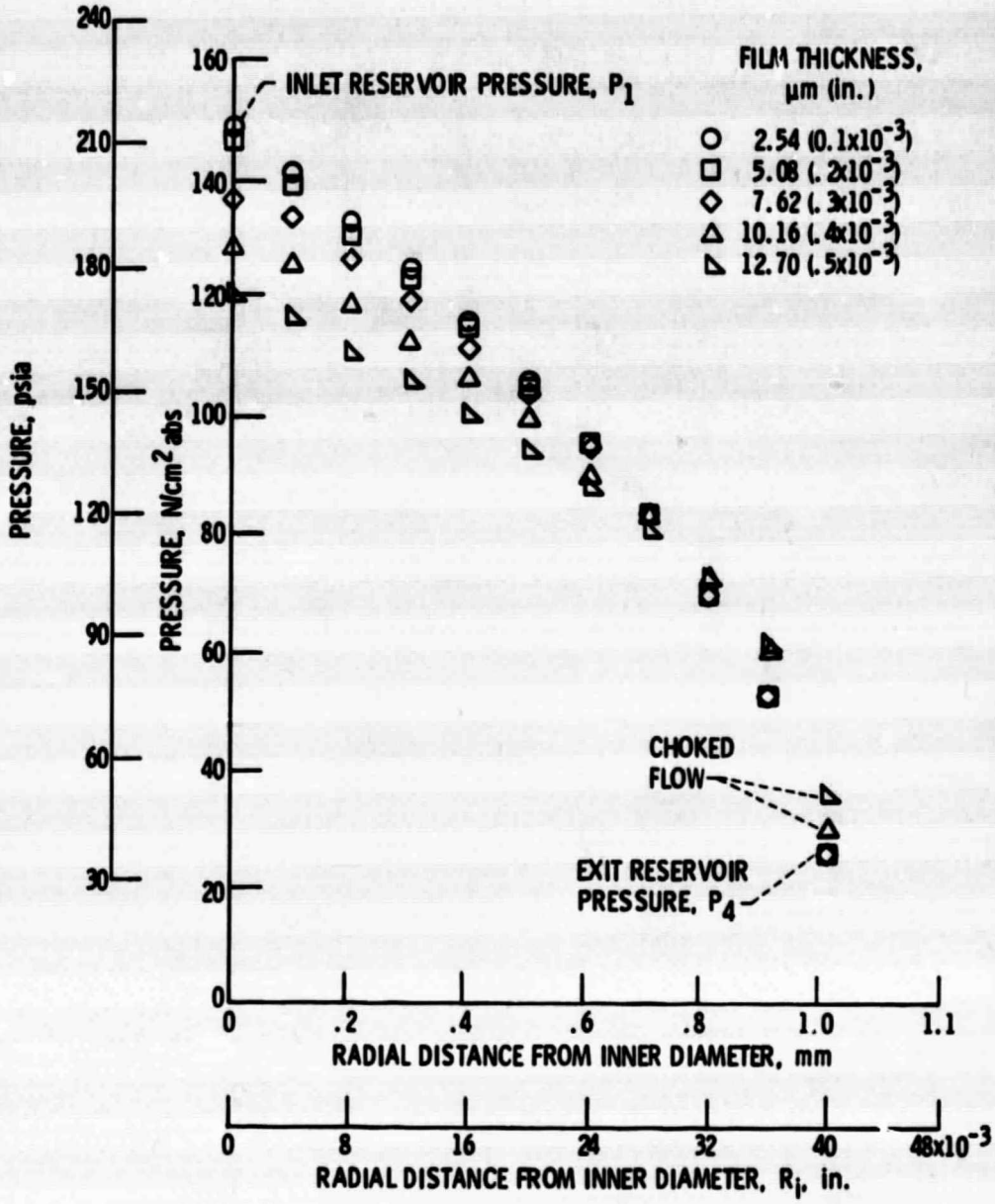

Figure 15. - Calculated radial pressure gradient across primary seal. Seal diameter, 6.44 cm (2.5 in.); sealed gas temperature, 672 K (750° F); spring force, 31.1 N (7.0 lbf); sliding speed, 192 m/s (650 ft/s); assumed inlet coefficient, 0.6.

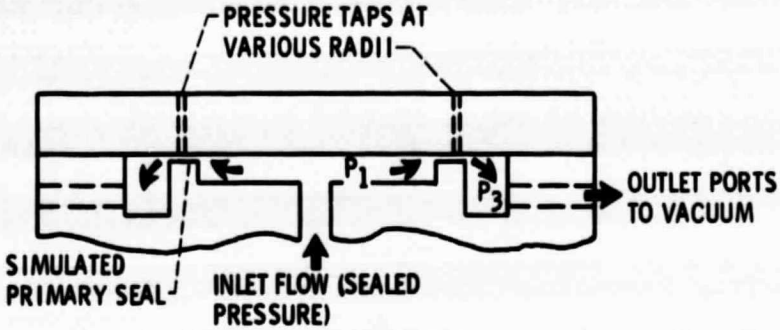

Figure 16. - Schematic of test rig for measurement inlet effect and pressure gradient across the primary seal.

E-9446

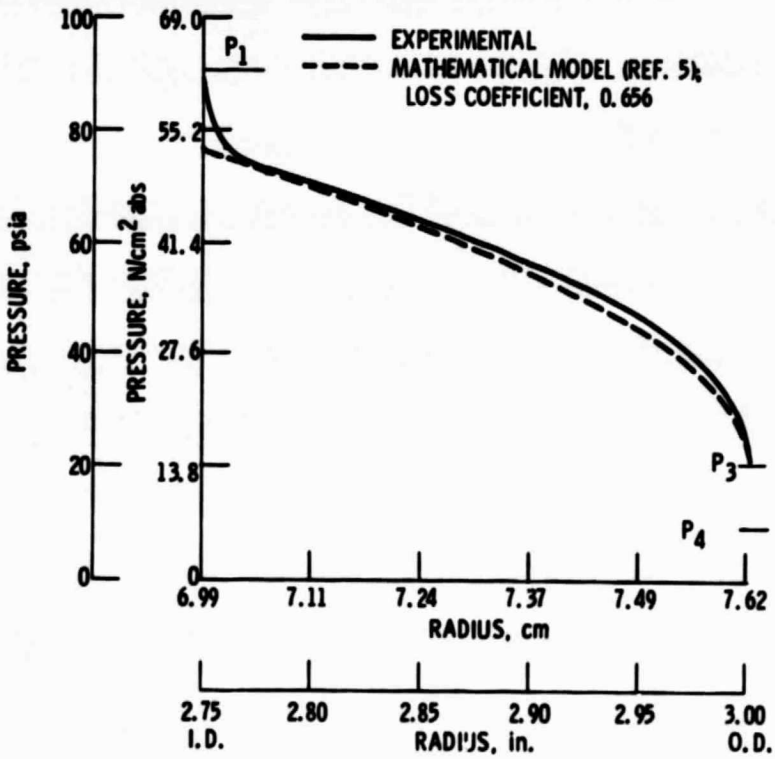

Figure 17. - Primary seal inlet pressure drop and pressure gradient. Sealed pressure, 62.3 N/cm² abs (90.4 psia); pressure ratio, ~10; sealing gap, h, 0.0028 cm (0.0011 in.); parallel seal faces.

ORIGINAL PAGE IS
OF POOR QUALITY

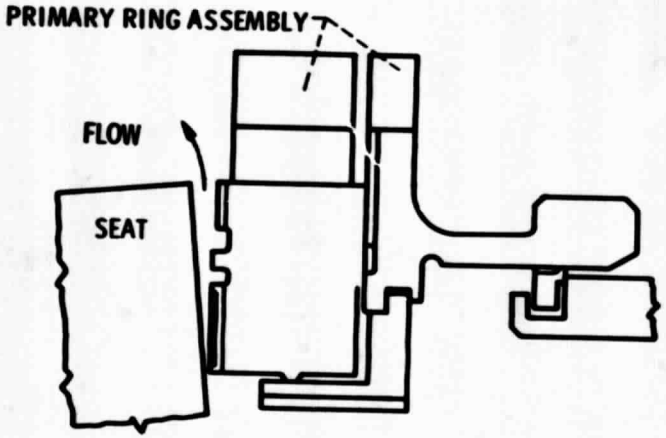

Figure 18. - Axisymmetric coning displacement of seat, causing nonparallel faces in primary seal and in self-acting geometry.

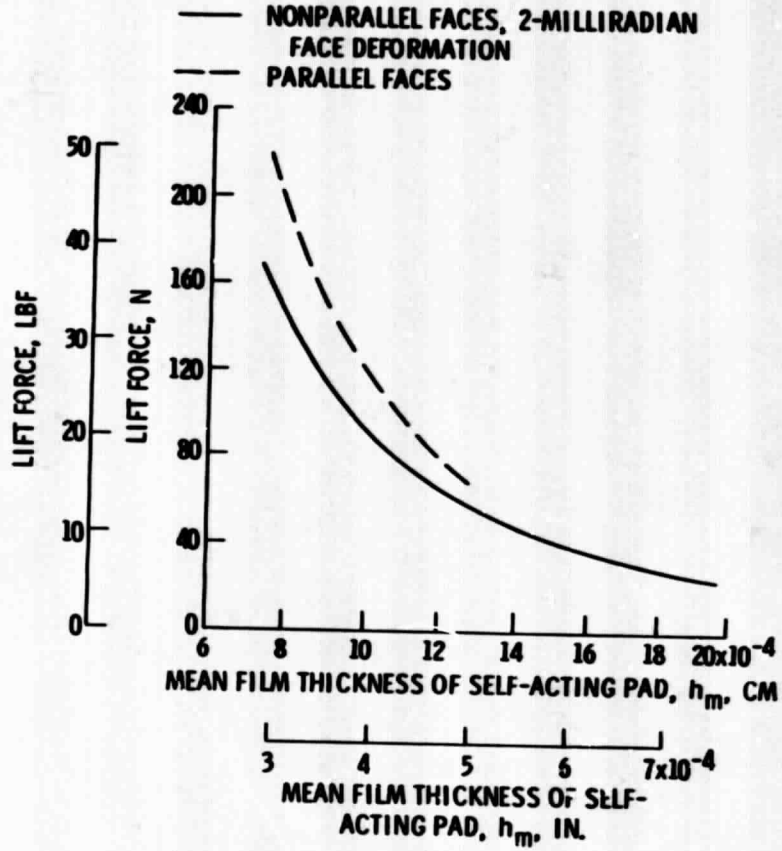

Figure 19. - Lift force of self-acting geometry. Number of pads, 20; pad depth, 0.0025 centimeter (0.001 in.); fluid, air. Sealed pressure, 148 N/cm^2 abs (215 psia); sliding speed, 153 meters per second (500 ft/sec); fluid temperature, 700 K (800° F).

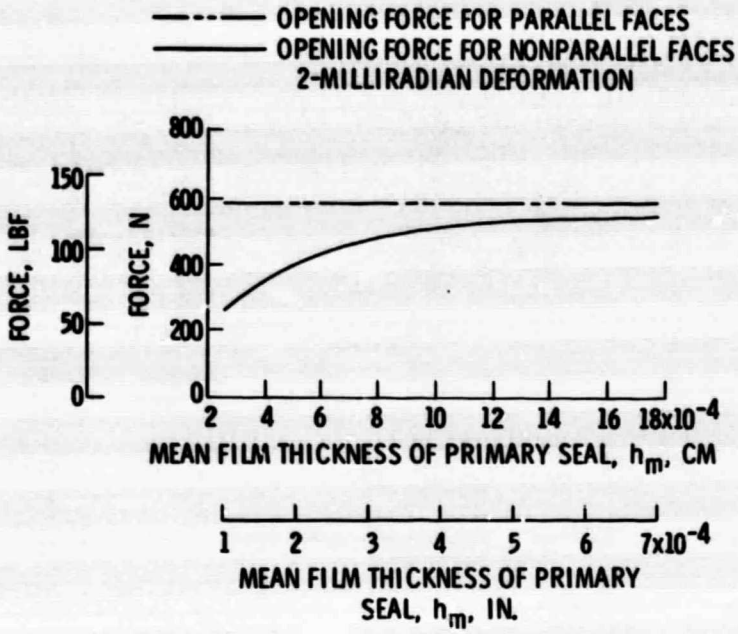

Figure 20. - Opening force acting on primary ring assembly. Sealed fluid, air. Sealed pressure, 148 N/cm^2 (215 psia); fluid temperature, 700 K (800^0 F). (From ref. 9.)

E-9446

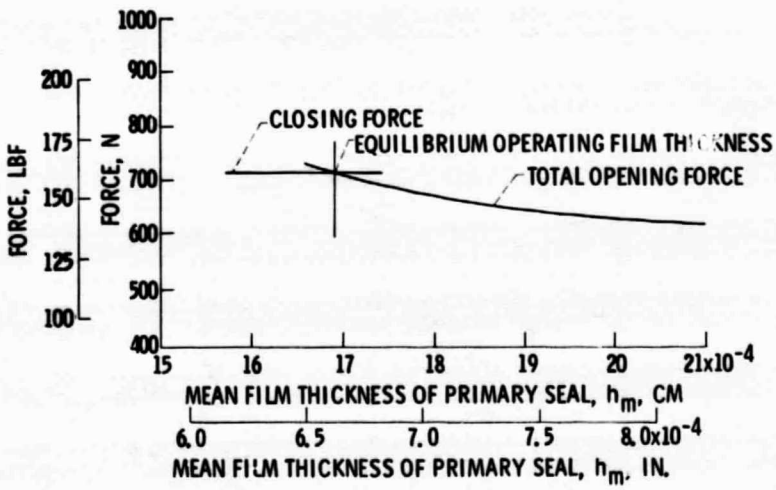

Figure 21. - Equilibrium gas film thickness as determined by total opening and closing forces for 2-millirad an face deformation. Sliding speed, 153 meters per second (500 ft/sec); sealed pressure, 148 N/cm^2 abs (215 psia); sealed gas temperature, 700 K (800^0 F).

ORIGINAL PAGE IS
OF POOR QUALITY

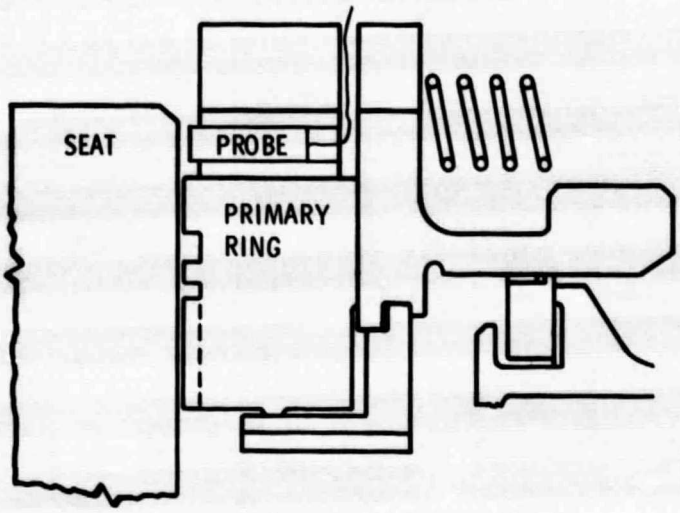

Figure 22. - Schematic showing priximity probe location.

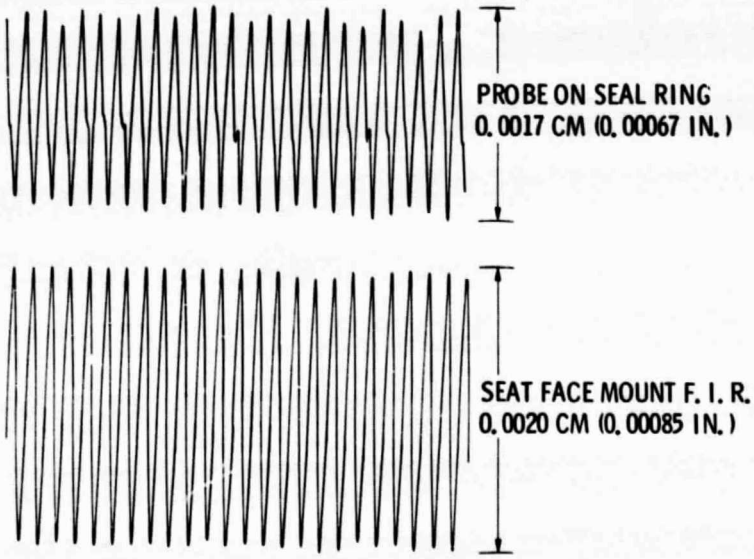

Figure 23. - Oscillograph traces showing response of ring to seat face runout. Recess-pad length to land-length ratio, 2:1; recess-pad depth, 0.0013 centimeter (0.0005 in.); sliding velocity, 61 meters per second (200 ft/sec); ambient pressure, 10 newtons per square centimeter (14.7 lb/in.^{2}); room temperature, 300 K (80^0 F); spring load, 1.13 kilograms (2.50 lb). (From ref. 13.)

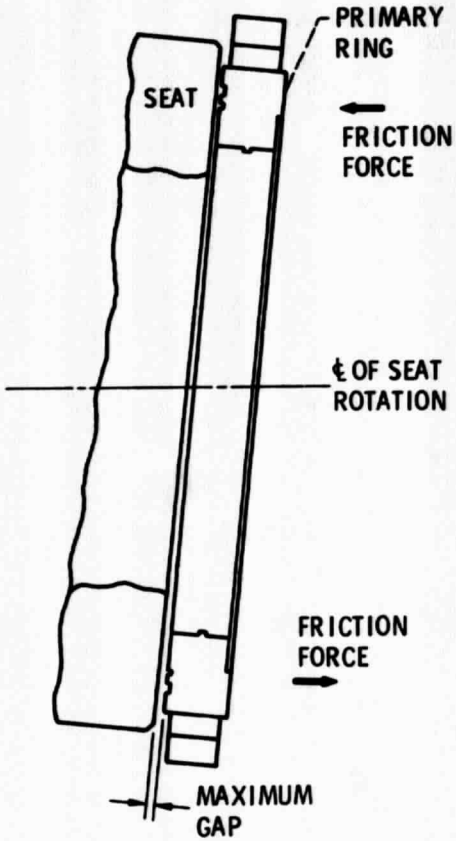

Figure 24. - Angular misalignment of sealing faces, nonaxisymmetric sealing gap.

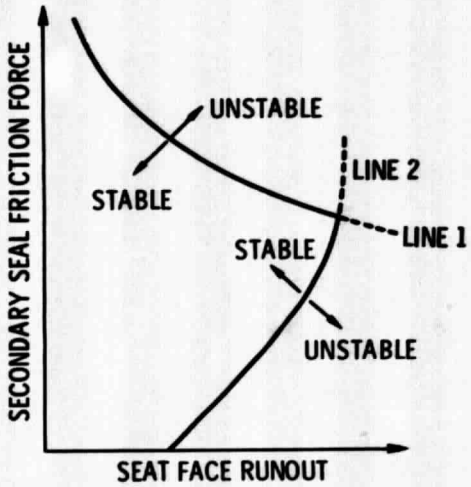

Figure 25. - Typical stability map of primary ring response to seat face runout.

ORIGINAL PAGE IS
OF POOR QUALITY

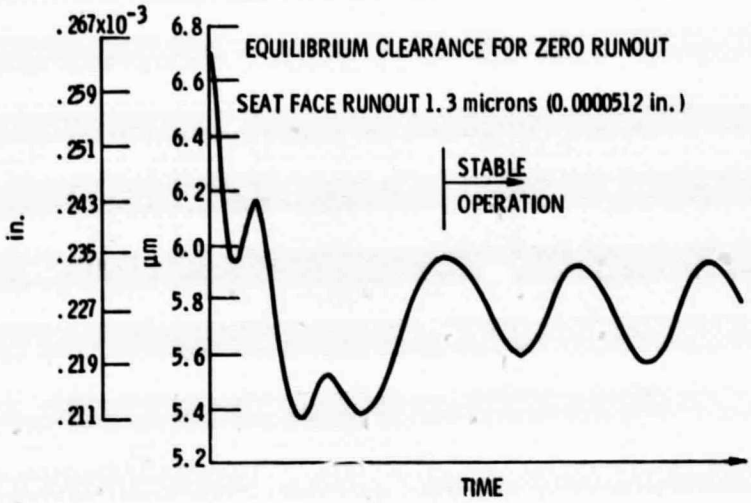

Figure 26. - Minimum clearance from start-up (time = 0) for 6.44 cm (2.5 in.) nominal diameter seal; sliding speed, 244 m/sec (800 ft/sec).

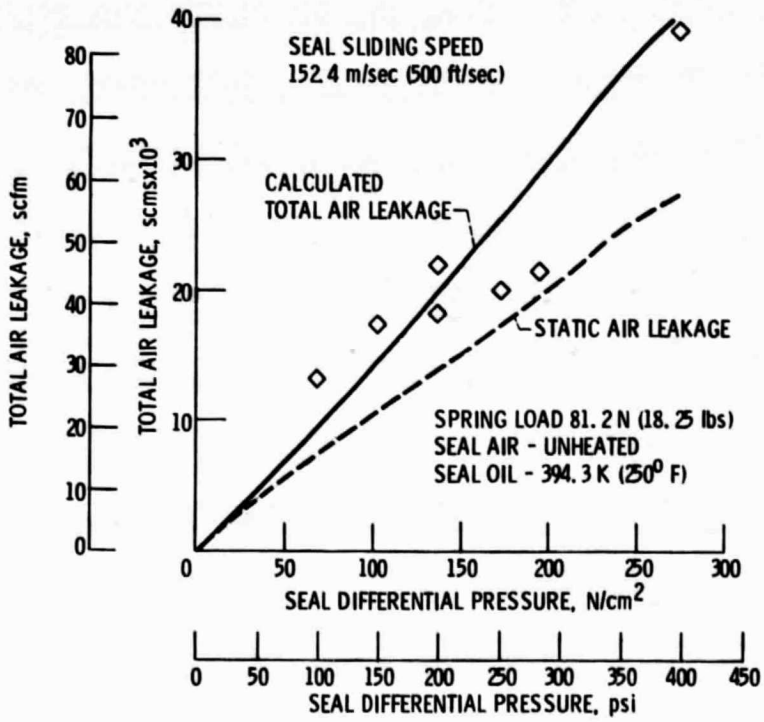

Figure 27. - Seal leakage; 16.76 cm (6.6 in.) nominal diameter seal. (Ref. 15.)

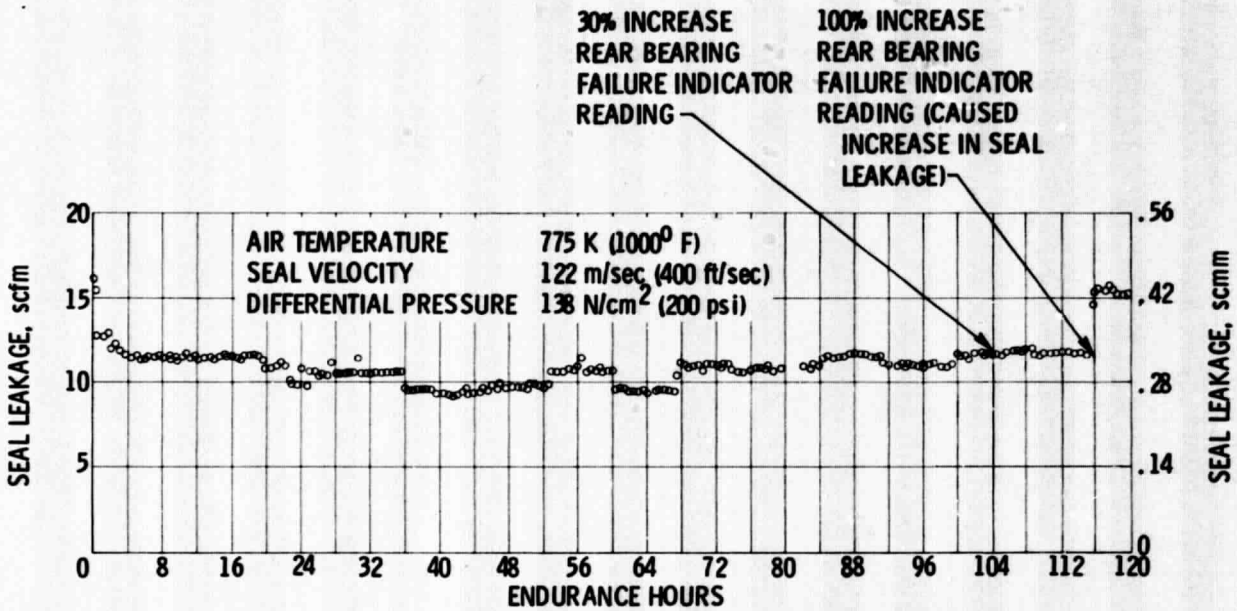

Figure 28. - Air leakage for 120-hour endurance test of 16.76 cm (6.6 in.) nominal dia seal (ref. 15).

ORIGINAL PAGE IS
OF POOR QUALITY

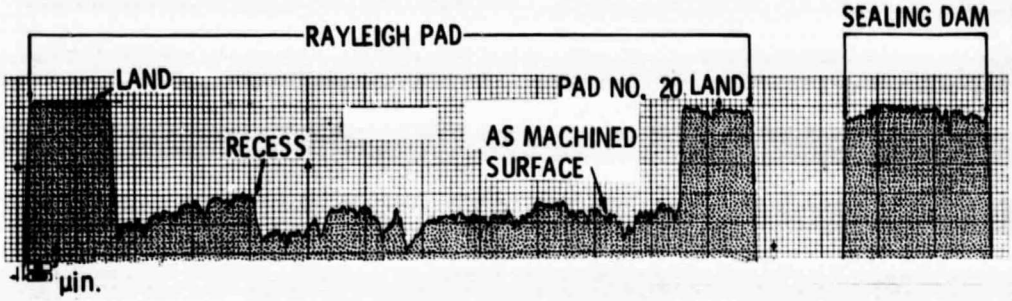

(a) AFTER 120 hr OF ENDURANCE.

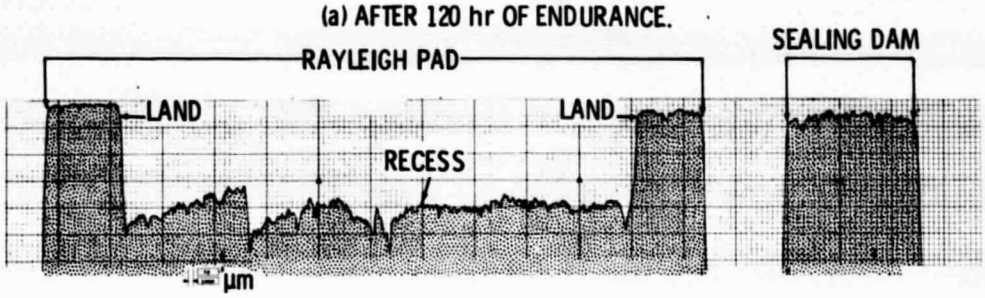

(b) AFTER 200 hr OF ENDURANCE; TOTAL TIME n SEAL 338.5 hr.

Figure 29. - Representative profile trace radially across a Rayleigh pad and primary seal after 200 hours of endurance. Total time on seal 338.5 hours. (From ref. 15.)

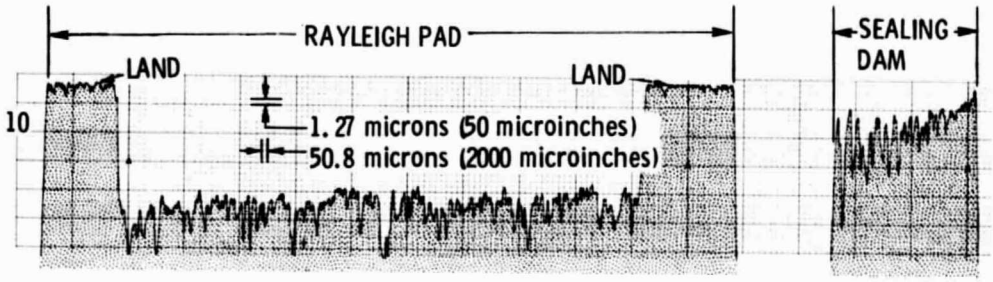

Figure 30. - Representative profile trace taken radially across the face of the carbon ring at completion of air entrained dirt test. Total test time, 14.5 hours.

E-9446

E-9446

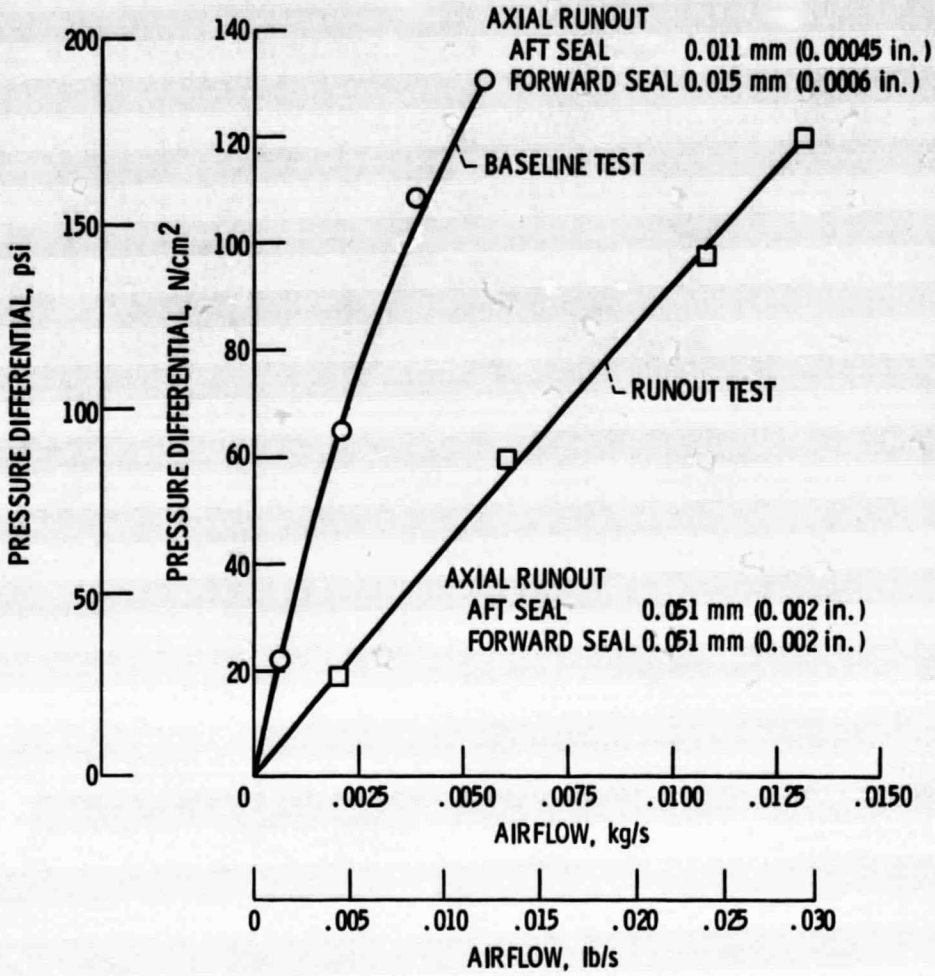

Figure 31. - Airflow through two seals as function of pressure differential at 145 m/s (475 ft/s) for seat face axial runout testing (ref. 16).

ORIGINAL PAGE IS
OF POOR QUALITY

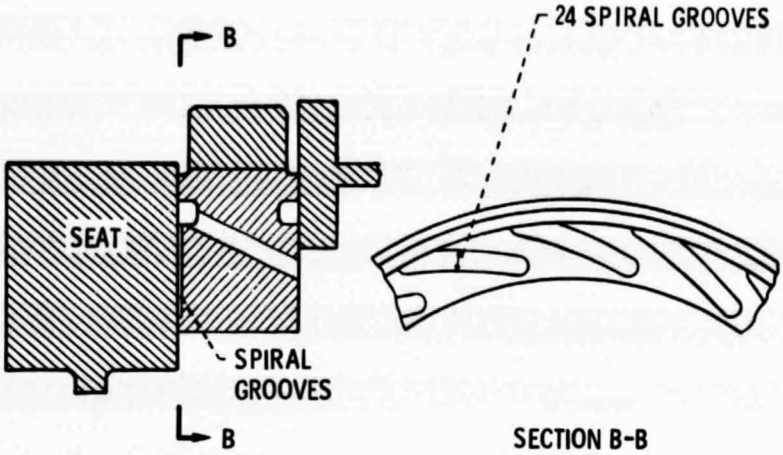

Figure 32. - Spiral groove self-acting seal.

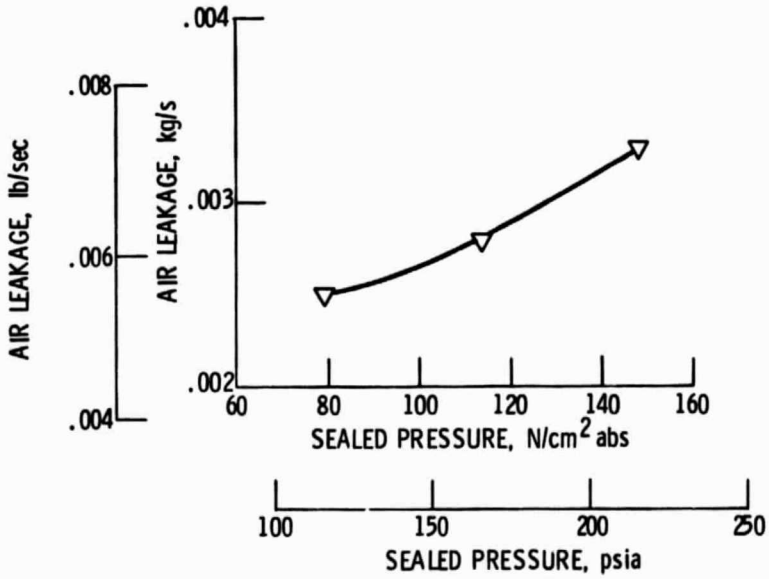

Figure 33. - Spiral groove self-acting seal; air leakage versus sealed pressure; sliding speed 182.9 m/s (600 ft/sec); 2 seals.

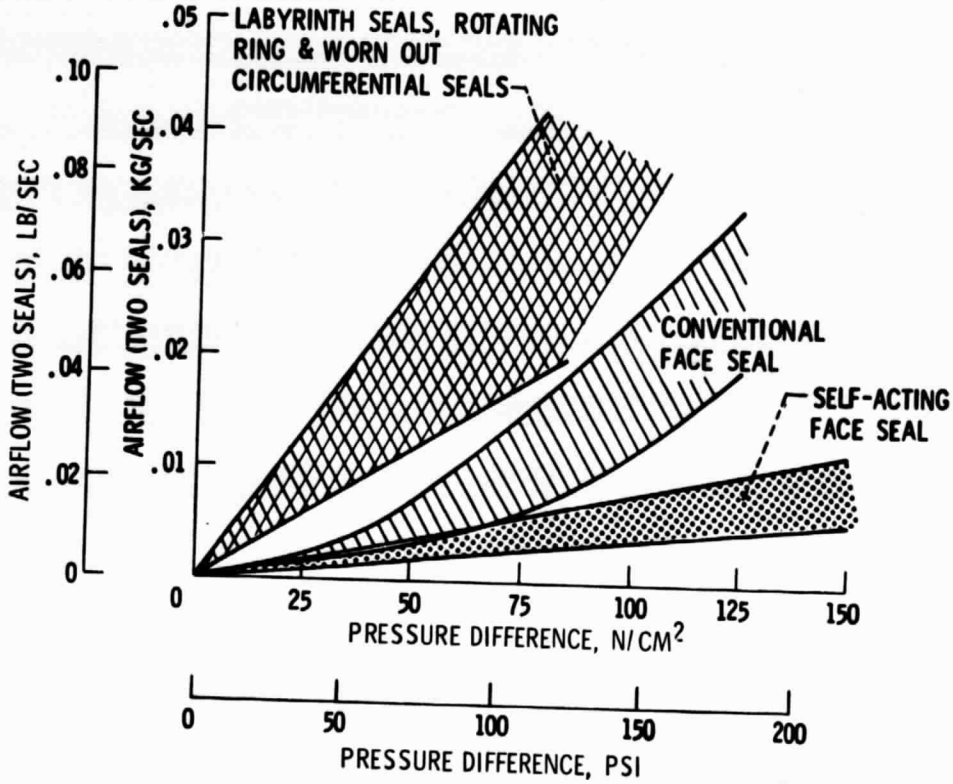

Figure 34. - Comparison of seal configurations.

E-9446

ORIGINAL PAGE IS
OF POOR QUALITY